Quaternary Science Reviews 237 (2020) 106302

Contents lists available at ScienceDirect

Quaternary Science Reviews

journal homepage: www.elsevier.com/locate/quascirev

Invited review

# Palaeoclimate perspectives on the Indian Ocean Dipole

Nerilie J. Abram [a, b, *], Jessica A. Hargreaves [a, b], Nicky M. Wright [a, b], Kaustubh Thirumalai [c], Caroline C. Ummenhofer [d, e], Matthew H. England [e, f]

[a] Research School of Earth Sciences, The Australian National University, Canberra, ACT, 2601, Australia
[b] ARC Centre of Excellence for Climate Extremes, The Australian National University, Canberra, ACT, 2601, Australia
[c] Department of Geosciences, University of Arizona, Tucson, AZ, 85721, USA
[d] Department of Physical Oceanography, Woods Hole Oceanographic Institution, Woods Hole, MA, 02543, USA
[e] ARC Centre of Excellence for Climate Extremes, University of New South Wales, NSW 2052, Australia
[f] Climate Change Research Centre, University of New South Wales, NSW, 2052, Australia

ARTICLE INFO

*Article history:*
Received 24 December 2019
Received in revised form
3 April 2020
Accepted 3 April 2020
Available online 3 May 2020

*Keywords:*
Indian Ocean Dipole (IOD)
Palaeoclimate
Climate variability and impacts
Last Millennium
Holocene
Last Glacial Maximum

ABSTRACT

The Indian Ocean Dipole (IOD) has major climate impacts worldwide, and most profoundly for nations around the Indian Ocean basin. It has been 20 years since the IOD was first formally defined and research since that time has focused primarily on examining IOD dynamics, trends and impacts in observational records and in model simulations. However, considerable uncertainty exists due to the brevity of reliable instrumental data for the Indian Ocean basin and also due to known biases in model representations of tropical Indian Ocean climate. Consequently, the recent Intergovernmental Panel on Climate Change (IPCC) report on the Ocean and Cryosphere in a Changing Climate (SROCC) concluded that there was only *low confidence* in projections of a future increase in the strength and frequency of positive IOD events.

This review examines the additional perspectives that palaeoclimate evidence provides on IOD trends, variability, interactions with the El Niño–Southern Oscillation (ENSO), and impacts. Palaeoclimate data show that recent trends towards more frequent and intense positive IOD events have been accompanied by a mean shift toward a more positive IOD-like mean zonal SST gradient across the equatorial Indian Ocean (due to enhanced warming in the west relative to the east). The increasing frequency of positive IOD events will imminently move outside of the range of natural variability in the last millennium if projected trends continue. Across a range of past climate states, periods of a mean positive IOD-like state in the Indian Ocean have been accompanied by elevated IOD variability. This includes events that exceed the magnitude of even the strongest measured historical events, demonstrating that the Indian Ocean can harbour even stronger variability than what has been observed to date. During the last millennium there has been a tight coupling between the magnitude of interannual IOD and ENSO variability, although positive IOD events have frequently occurred without any indication of a co-occurring El Niño event. This IOD–ENSO coupling may not have persisted across past climates that were very different from the present, raising questions of whether their interaction will change in a rapidly warming future. Palaeoclimate evidence for hydroclimate changes during the last millennium further points to the importance of interannual IOD and ENSO variability in providing the rainfall that breaks droughts in regions that are impacted by these modes of variability. Overall, this review highlights the rich insights into the IOD that can be gained from palaeoclimate evidence. Palaeoclimate data helps to overcome known limitations in observations and model simulations of the IOD, and demonstrates that strong conclusions about the IOD and its impacts can be reached when the evidence for past, present and future behaviour of the IOD are assessed together.



## 1. Introduction

The Indian Ocean Dipole (IOD) is a form of interannual climate variability in the tropical Indian Ocean (Cai et al., 2013, 2019; Saji et al., 1999; Webster et al., 1999; Fig. 1). Positive IOD events are

* Corresponding author. Research School of Earth Sciences, The Australian National University, Canberra, ACT, 2601, Australia.
*E-mail address:* nerilie.abram@anu.edu.au (N.J. Abram).

https://doi.org/10.1016/j.quascirev.2020.106302
0277-3791/

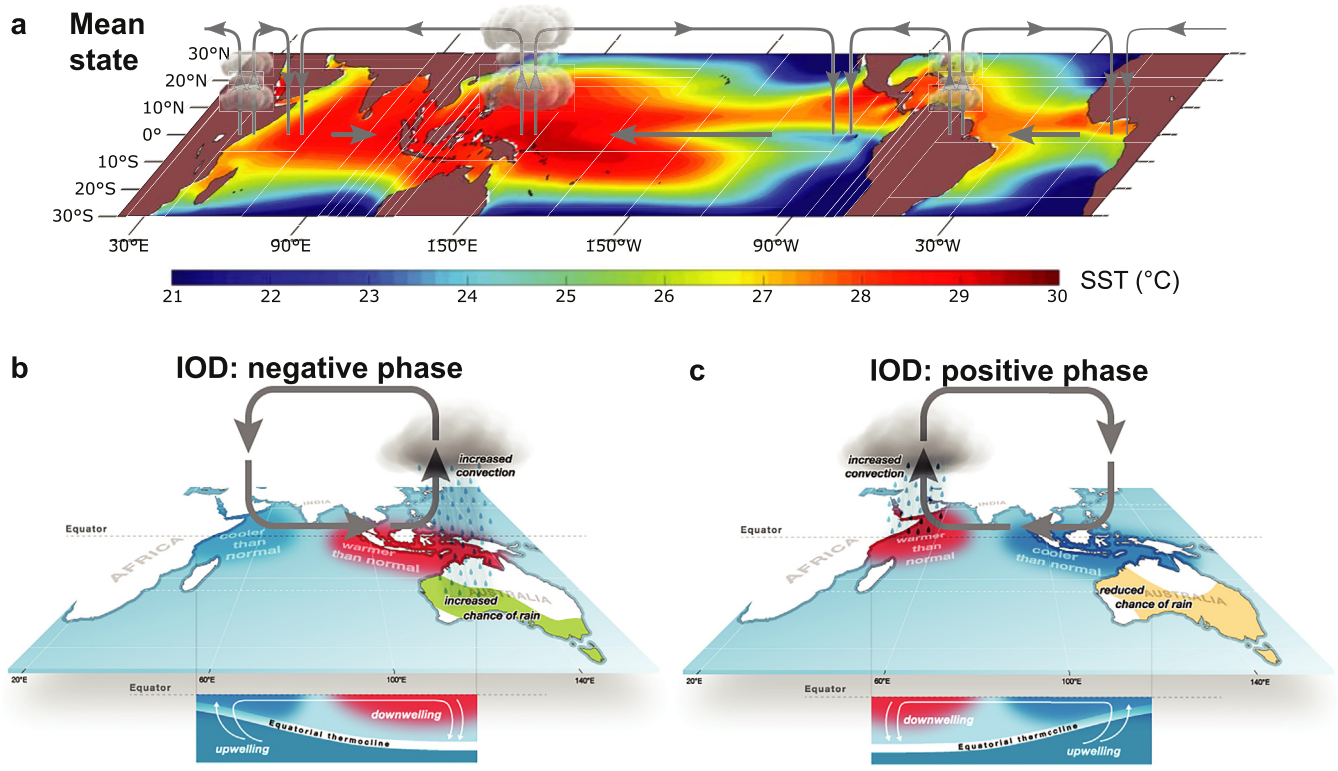


**Fig. 1. The Indian Ocean Dipole**. (a) Background mean state of tropical SST (shading) and Walker circulation (arrows). Image after (Cai et al., 2019). (b–c) Schematic of ocean-atmosphere anomalies associated with negative and positive Indian Ocean Dipole events. Source: Australian Bureau of Meteorology; http://www.bom.gov.au/climate/iod/.

initiated by the development of enhanced ocean upwelling along the Java and Sumatra coasts in the eastern Indian Ocean. This generates anomalously cool sea surface temperatures (SSTs) in the eastern Indian Ocean, resulting in strengthened easterly winds along the Equator, enhanced ocean warming in the western Indian Ocean and an associated increase (decrease) in atmospheric convection over the western (eastern) tropical Indian Ocean (Webster et al., 1999; Fig. 1c). IOD activity is seasonally phase locked by the wind reversals associated with the Asian-Australian monsoons. Positive events begin to develop around May–June as southeasterly trade winds form in the tropical eastern Indian Ocean, and once established, ocean–atmosphere feedbacks are able to sustain and strengthen positive IOD anomalies until the reversal of the trade winds in October–November cause events to peak and then rapidly dissipate (Cai et al., 2013; Webster et al., 1999).

The IOD causes worldwide impacts, which are particularly severe in the regions surrounding the Indian Ocean basin (Cai et al., 2013; Han et al., 2014; Saji et al., 1999; Webster et al., 1999). IOD variability is implicated in Australia's worst droughts (Ummenhofer et al., 2009a), and positive IOD events increase fire risk in southeast Australia in the following austral summer (Cai et al., 2009a). Positive IOD events have been associated with severe wildfires and habitat destruction in Indonesia (Abram et al., 2003; Webster et al., 1999), and bring risks to food security through impacts on crop yields across India, China, East Africa and southeast Australia (Anderson et al., 2019). Positive IOD events have also been linked to floods and disease outbreaks in East Africa (Birkett et al., 1999; Epstein, 1999; Hashizume et al., 2012; Linthicum et al., 1999; Webster et al., 1999). Negative IOD events involve a strengthening of the zonal SST gradient (warming in the East, cooling in the West; Fig. 1b). They are not as well characterised and tend to be weaker than their positive IOD event counterparts (Cai and Qiu, 2012; Cai et al., 2013), but the strongest negative IOD event on record in 2016 caused extreme drought in eastern Africa and heavy rainfall in Indonesia and Australia (Lim and Hendon, 2017).

The IOD was first formally defined in 1999, following the extreme positive IOD events of 1994 and 1997 (Saji et al., 1999; Webster et al., 1999), although it was previously recognised that the Indian Ocean might be capable of harbouring ocean–atmosphere modes similar to the other basins (Anonymous, 1994; Hastenrath et al., 1993; Nicholls, 1989; Tourre and White, 1995). Twenty-years of subsequent research has provided a range of observational evidence for the characteristics of IOD variability and impacts, as well as projections for how the IOD is expected to change in the future. However, considerable uncertainties remain: the reliable instrumental SST history for the tropical Indian Ocean is short, with long-term SST products suffering from measurement biases and lack of input data prior to the mid-20th Century (Chan et al., 2019; Gopika et al., 2019). Some global SST products also fail to capture the full magnitude of coastal upwelling anomalies in the eastern Indian Ocean during positive IOD events, even for well-observed recent decades (Abram et al., 2007). The brevity of reliable SST observations hampers the ability to resolve whether the IOD is an independent mode relative to the tropical El Niño–Southern Oscillation (ENSO) (Stuecker et al., 2017; Wang et al., 2019; Zhao and Nigam, 2014), and precludes knowledge of the full range of potential variability of the IOD (Cai et al., 2019). Models are also known to have biases in their representation of the IOD. Models typically produce IOD variability that is stronger with more frequent events than is indicated by observational data (Weller and Cai, 2013), owing to an unrealistic representation of the mean state of the zonal thermocline slope across the equatorial Indian Ocean that results in an overly strong thermocline-SST feedback (Cai and Cowan, 2013). Biases between models in their spatial

representation of ENSO and IOD variability (Bellenger et al., 2014; Cai et al., 2018; Taschetto et al., 2014) may also impact assessments of future changes in IOD variability and its impacts (Brown et al., 2016).

Assessments by the Intergovernmental Panel on Climate Change (IPCC) of the scientific evidence for climate change, and its effects on climate modes such as the IOD, are built upon multiple lines of evidence (Mach et al., 2017), including evidence from palaeoclimate archives (Masson-Delmotte et al., 2013). Palaeoclimate records can help to substantiate findings based on short observational data by providing a long-term context in which to view current anthropogenic climate changes, or to validate model simulated outcomes by assessing past climates across a range of different background climate states. IOD research to date has been primarily based on observational and model-derived data, but given the known limitations of these lines of evidence there is an important role for palaeoclimate perspectives to play in scientific understanding of the IOD.

In this review we provide an assessment of the perspectives that palaeoclimate data contribute to key aspects of past, present and future IOD variability. We first review the characteristics of Indian Ocean variability in light of 20 years of additional high-quality observations since the IOD was first defined (Section 2). This gives important context for interpreting palaeoclimate evidence of the IOD, but is not designed as an in-depth review of modern day Indian Ocean climate dynamics (e.g. see Schott et al., 2009, for this type of review). We then assess the palaeoclimate evidence for trends in the IOD (Section 3) and IOD variability (Section 4) across a range of timescales spanning from the 20th Century to the Last Glacial Maximum (LGM). Finally, we review the evidence that palaeoclimate data provides on IOD–ENSO interactions (Section 5), and their impacts (Section 6). Our review focuses primarily on the more well-studied positive phase of the IOD (Fig. 1c), as these events tend to be larger in magnitude, are associated with more widespread impacts, and produce the clearest signals in available palaeoclimate data.

## 2. Defining Indian Ocean variability

Before assessing palaeoclimate evidence of the IOD and its impacts, it is important to first review key aspects of IOD variability in observational data and the implications that this has for interpreting the palaeoclimate archive. Variability of the IOD is most commonly defined based on the Dipole Mode Index (DMI), with instrumental data generally assumed to be reliable since 1958, following the approach of Saji et al. (1999). The DMI is based on the difference in SST anomalies between the equatorial western Indian Ocean (10°S–10°N, 50°E–70°E) and the southeastern Indian Ocean (10°S–equator, 90°E–110°E) (Saji et al., 1999). It was later proposed that the western DMI region should be shifted to 10°S–10°N, 60°E–80°E (Saji and Yamagata, 2003), however this has not been widely adopted and the original definition remains the most commonly used index of IOD variability. There is no single method for how to use the DMI to determine the occurrence of IOD events, but generally it involves the index exceeding a given threshold for a certain length of time. For example, the Australian Bureau of Meteorology defines a positive IOD event as occurring when the weekly DMI remains above +0.4 °C for at least eight consecutive weeks (http://www.bom.gov.au/climate/iod/).

The additional 20 years of high-quality SST data since the DMI was first defined allows us to reassess the characteristics of Indian Ocean variability and the suitability of the DMI for defining this variability. We do this by first using an Empirical Orthogonal Function (EOF) analysis of SST anomalies (using OISSTv2 data; January 1982 to December 2019) in the Indian Ocean basin (Fig. 2). The geographic configuration of the Indian Ocean differs from other ocean basins. Specifically, the continental landmass that borders the northern margin of the ocean results in a strong monsoon climate that imparts a seasonally reversing wind structure on the basin (Schott et al., 2009). This means that it is of critical importance to assess the features of Indian Ocean variability through a seasonally-specific lens.

Here, we perform the EOF analysis using half-yearly means for July–December and January–June. These half-year definitions are designed to capture the SST anomalies associated with positive IOD events (which are strongest between July–December), and acknowledging that chronological limitations exist in (coral-based) palaeoclimate data (Abram et al., 2020), precluding the finer-scale temporal analysis that is possible for instrumental data and model output. We do note that repeating the EOF analysis using traditional 3-month seasons results in similar patterns for June–August and September–November as discussed here for July–December. Likewise, EOF patterns for December–February and March–May have similar characteristics to the January–June half year reported here.

The first two EOFs of July–December SST variability in the Indian Ocean display an IOD-like structure (Fig. 2a–c). EOF1 displays the well described zonal SST anomaly patterns of cooling in the east and warming in the west indicative of a reduced or even reversed zonal SST gradient (Fig. 2a). Positive anomalies in the principal component (PC) of this EOF1 generally coincide with years classified as positive IOD events. The second EOF (Fig. 2b) also displays a reduced zonal SST gradient due to cooling in the upwelling region of the eastern Indian Ocean, and again positive anomalies in the principal component tend to coincide with positive IOD event years. However, in the second EOF the focus of the contrasting warm SST anomalies is in the central subtropical Indian Ocean and there is essentially no signal in the western DMI region. The eastern cooling anomaly also occurs over a broader region into the subtropics (i.e. it is not restricted just to the eastern coastal upwelling region). The spatial structure of EOF2 is similar to the meridional gradient of SST anomalies that have been described as having the strongest rainfall impact in southern Australia (England et al., 2006; Nicholls, 1989; Ummenhofer et al., 2009a, 2009b), but EOF2 is inconsistent in location or season with descriptions of a possible Indian Ocean Subtropical Dipole (Behera and Yamagata, 2001; Morioka et al., 2010; Yuan et al., 2014). It is possible that EOF1 and EOF2 may represent modified “flavours” of IOD variability, in a similar way to how central and eastern Pacific-type manifestations of El Niño variability are known for the Pacific Ocean (Ren and Jin, 2011).

Overall, the EOF analysis confirms that the IOD is the dominant mode of Indian Ocean variability during the July–December interval, and that the bounds of the eastern DMI region are well-located to capture anomalies of IOD variability. However, it also indicates that the western DMI box may not be optimally located. A region spanning approximately 30–10°S, 60–90°E would better capture the warm SST pole of positive IOD events in the first two EOFs, or may be useful in conjunction with the traditional western DMI region for differentiating between EOF1 and EOF2 type IOD events.

The dominant pattern of Indian Ocean variability in the January–June interval (Fig. 2d–f) is the widespread warming of the Indian Ocean Basin Mode (IOBM) (Taschetto et al., 2011). The IOBM is not considered as a mode of variability, but rather a forced response to ENSO processes in the Pacific (Taschetto et al., 2011). Both the eastern and western DMI regions experience warming in January–June associated with EOF1, and the principal component of this EOF demonstrates the association of positive IOBM conditions with El Niño events in the Pacific Ocean (Fig. 2d, f). The

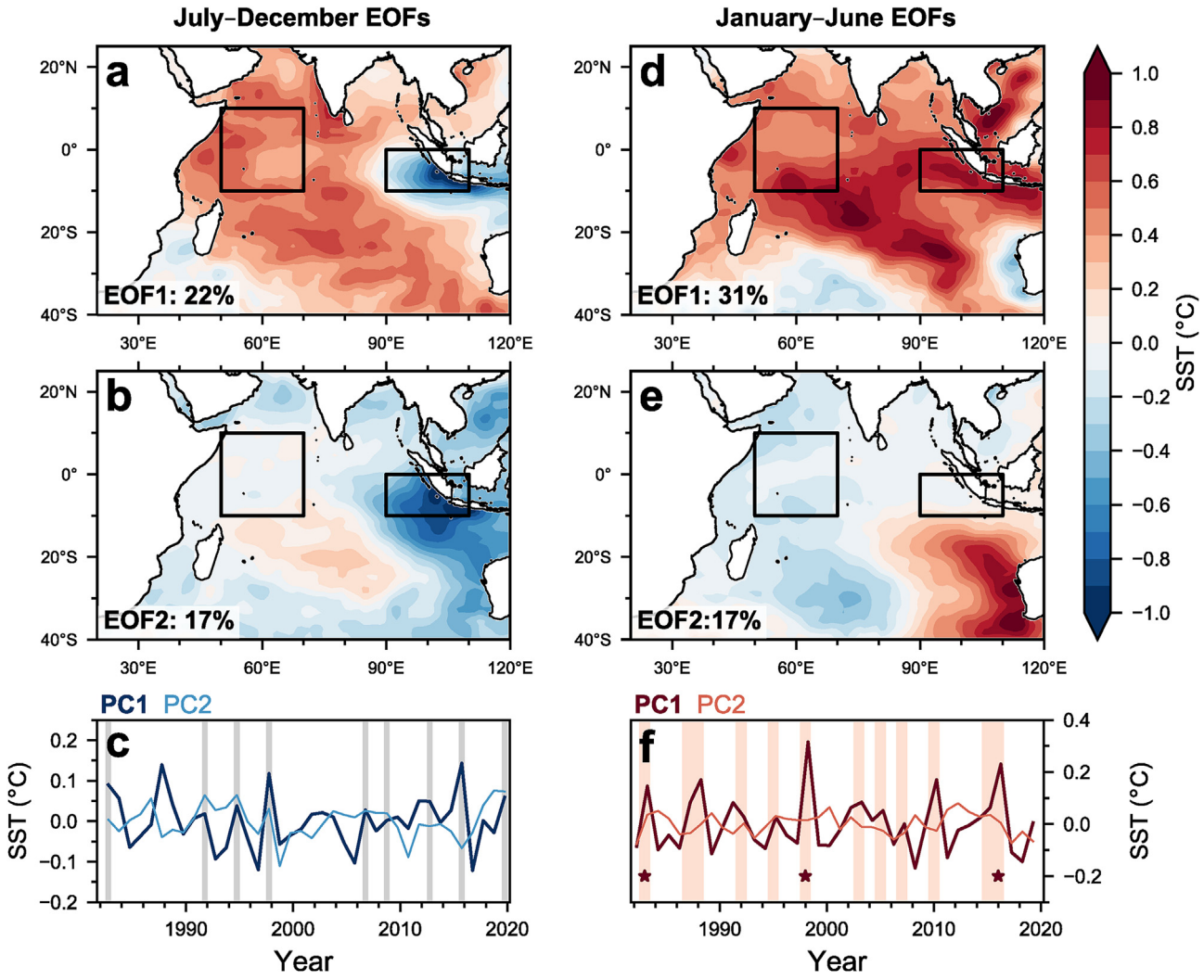


**Fig. 2. Dominant patterns of interannual SST variability in the Indian Ocean**. EOF analysis was carried out on detrended OISSTv2 SST data (January 1982–December 2019; Reynolds et al., 2002) for the region spanning 40°S–25°N, 20°E–120°E. The first two EOF patterns are shown, along with time series of their principal components (PC). Owing to the strong seasonality of Indian Ocean climate, EOF analysis is performed on July–December (a–c) and January–June half-yearly (d–f) means. Black boxes on map panels (a–b, d–e) indicate the western and eastern regions used to define the Dipole Mode Index (Saji et al., 1999). Grey shading on panel c indicates positive IOD event years (see Fig. 4 for classification details). Red shading on panel f indicates El Niño event years, with stars indicating eastern Pacific-type El Niño events (as classified by Ren and Jin, 2011, and Freund et al., 2019).

July–December PC1 in Indian Ocean SSTs is also highly correlated with PC1 of the following January–June ($r = 0.65$, $p < 0.01$, $n = 37$), indicative of the previously noted covariation between IOD and ENSO variability (Stuecker et al., 2017; Wang et al., 2019; Zhao and Nigam, 2014). The second EOF of January–June Indian Ocean SST anomalies reflects subtropical variability, including that associated with the subtropical Ningaloo Niño that is prominent during La Niña events (Feng et al., 2013; Kataoka et al., 2014), and does not have an imprint on the tropical eastern or western DMI regions (Fig. 2e).

Exploration of SST time series for the eastern and western DMI regions (Fig. 3) builds upon the insights gained from the EOF analysis of Indian Ocean SST variability. Prominent SST cooling in the eastern DMI region is generally associated with years classified as positive IOD events. The magnitude of SST cooling during positive IOD events varies by SST product, with the 1° × 1° resolution OISSTv2 product (available since November 1981, based on satellite, ship and buoy observations; Reynolds et al., 2002) best capturing the full magnitude of coastal upwelling-induced cooling along the Java and Sumatra coasts (Fig. 3a). The 0.25° × 0.25° resolution version of the OISSTv2 product (also referred to as AVHRR; Banzon et al., 2016) displays very similar variability to the 1° × 1° resolution product, but has stronger long-term warming trends in the DMI regions (not shown in Fig. 3). The 2° × 2° resolution ERSSTv5 (Smith et al., 2008) and 1° × 1° resolution HadISST (Rayner et al., 2003) SST products are available over a longer period of time, but both fail to adequately capture the magnitude of ocean cooling in the eastern DMI region even during recent extreme positive IOD events (e.g. 1994, 1997, 2019 in Fig. 3a), suggesting that extreme caution should be used in examining IOD variability with these products.

In the eastern DMI region, rapid reversals from cool to warm SST anomalies are seen for positive IOD events that co-occur with El Niño events (e.g. the 1997/1998 sequence in Fig. 3a). This reflects the transition from July–December positive IOD event cooling to January–June IOBM warming seen in the eastern DMI region through the EOF analysis (Fig. 2). This characteristic seasonal anomaly pattern provides an opportunity to explore relationships

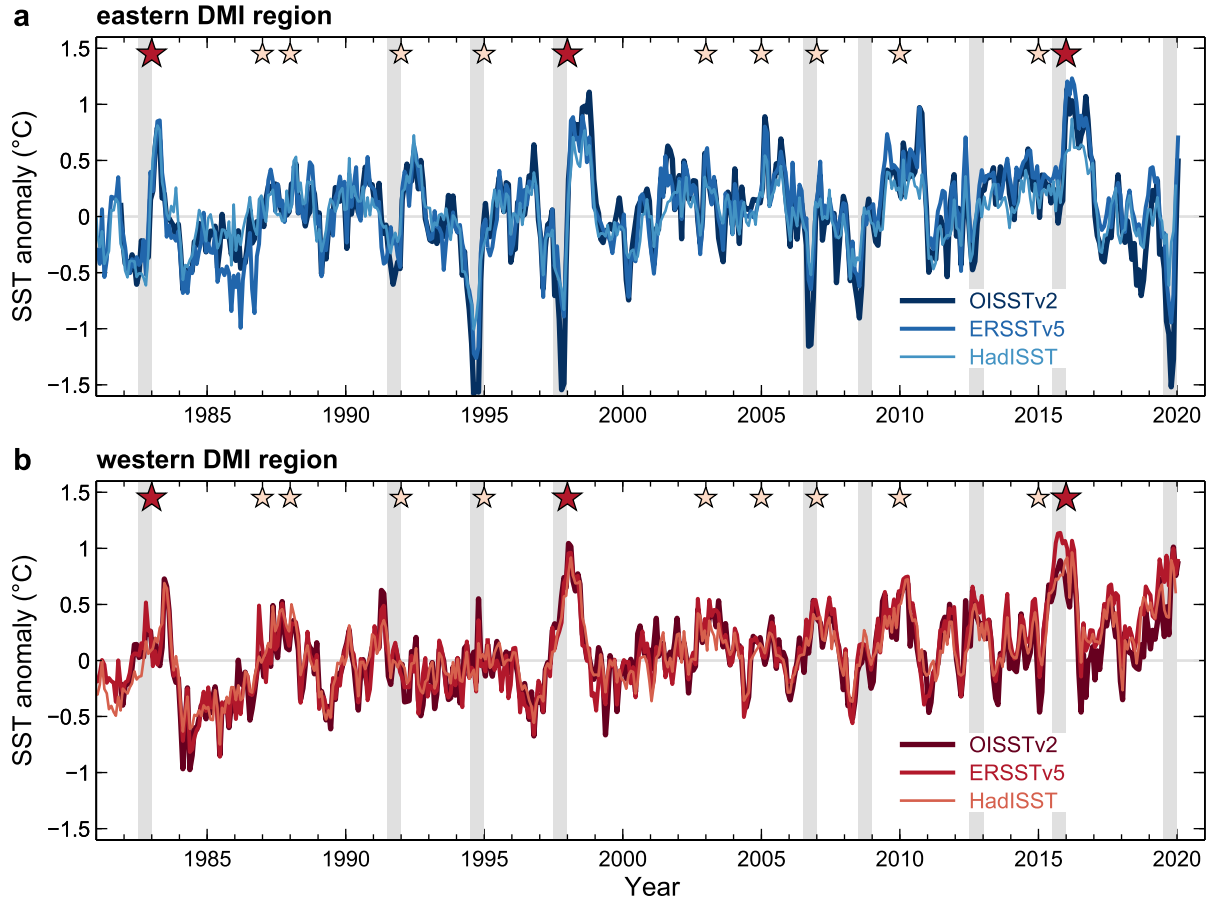


**Fig. 3. Time series of SST anomalies for the eastern and western DMI regions.** SST anomalies from different SST products are shown relative to 1981–2010 climatology and have not been detrended. Grey bars indicate July–December of positive IOD event years (see Fig. 4 for classification details), small orange stars indicate central-Pacific type El Niño events and large red stars indicate eastern-Pacific type El Niño events (as classified by Ren and Jin, 2011, and Freund et al., 2019). Data is shown at monthly mean resolution for the OISSTv2 (Reynolds et al., 2002), HadISST (Rayner et al., 2003), and ERSSTv5 (Smith et al., 2008) products.

between IOD and ENSO variability in the past (Section 5).

In the western Indian Ocean, the SST anomalies associated with IOD variability are more ambiguous as positive IOD events are not consistently characterised by anomalously warm SST (Fig. 3b). Instead, the years where strong warming is seen in the western DMI region are generally associated with El Niño conditions in the Pacific, with this connection appearing to be most pronounced for strong, eastern-Pacific type El Niño events (e.g. 1982/83, 1997/98, 2015/16 in Fig. 3b). In some cases, years that have previously been categorised as positive IOD events using the DMI (e.g. 1982, 2015) are seen to be dominated by the El Niño driven warming anomaly in the western region and lack anomalous ocean upwelling and cooling in the eastern region.

The dominance of ENSO-related anomalies in the western DMI region has been described in numerous observational studies, and removal of this ENSO-forced signal in Indian Ocean SSTs has been found to result in a residual monopole signal focused only on the eastern upwelling region (Zhao and Nigam, 2014). Other studies have also suggested that the eastern DMI region alone, rather than the west–east difference in SST anomalies, may be a better measure for defining IOD variability (Abram et al., 2015; Meyers et al., 2007). An eastern-only method of defining the IOD would require positive IOD events to display enhanced ocean upwelling and SST cooling, which is a fundamental physical process of IOD variability (Meyers et al., 2007; Zhao and Nigam, 2014), and could avoid false classification of positive IOD events due to the manifestation of El Niño-driven warming in the western and central Indian Ocean alone.

We next examine IOD variability based on three different indices (Fig. 4). These indices are: (i) the traditional DMI (difference in detrended SST anomalies in the western and eastern regions (Saji et al., 1999), (ii) a variant of the DMI using the difference in detrended SST anomalies between the central south tropical Indian Ocean (60–90°E, 10–30°S) based on our EOF analysis (Fig. 2), and (iii) an index based only on the eastern DMI region detrended SST anomaly (inverted for ease of comparison with the DMI) based on our findings from Fig. 3. All three versions of the IOD index show a high degree of covariance (Fig. 4a), and share equivalent spatial correlations with rainfall impacts (Fig. 4c, e, g). This comparison also demonstrates that SST anomalies in the eastern region dominate variability of the DMI. Detrended SST anomalies in the eastern IOD region explain 61% of the variance in the full monthly-resolution DMI and 87% of the July–December variability in the DMI, compared to 33% and 57% respectively for equivalent metrics of the contribution of the western region to the DMI.

The lack of an agreed methodology for classifying IOD events (e.g. level and duration of threshold exceedance, use of detrending and/or detrending method used, use of different SST products, etc.) means that there is no consistent established set of years that are classified as positive IOD event years (Abram et al., 2015; Cai et al., 2014b; Meyers et al., 2007; Saji et al., 1999; Saji and Yamagata, 2003; Ummenhofer et al., 2009a; Verdon-Kidd, 2018). Positive IOD event detection across the three IOD index variants in Fig. 4 is

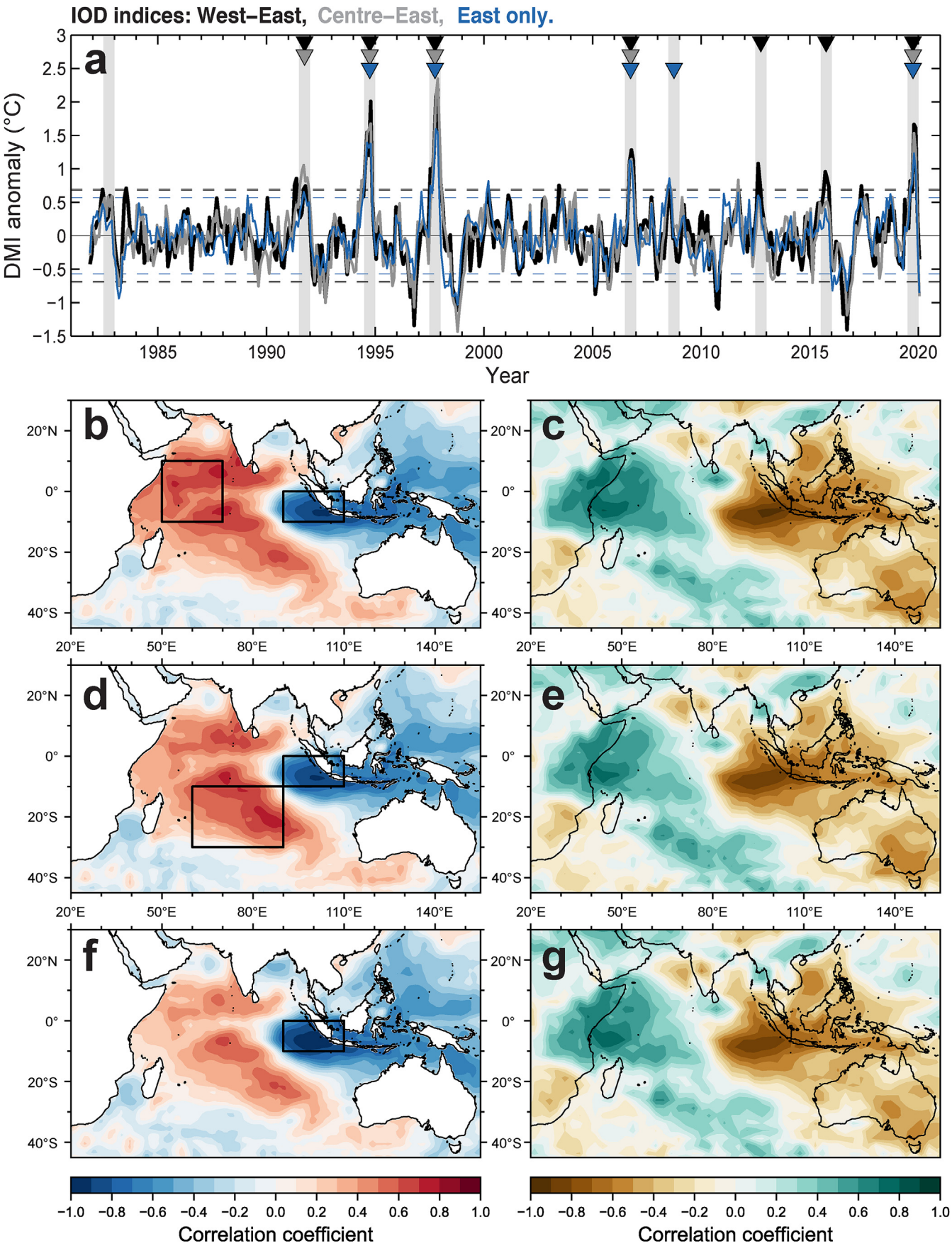
IOD indices: West–East, Centre–East, East only.
a
DMI anomaly (°C)
Year
b
c
d
e
f
g
Correlation coefficient
Correlation coefficient

based on the detrended monthly index exceeding the +1.5 standard deviation (σ) level (1981–2010 climatology) for at least 2 months during the July–December interval (Fig. 4). This replicates the event detection method applied to coral palaeoclimate data of IOD variability (Abram et al., 2008, 2020). Across the three variants of IOD indices examined here, our analysis suggests that since 1981, the most consistently defined positive IOD events are 1994, 1997, 2006, and 2019. These events are classified across all variants of the IOD indices and their classification is insensitive to the detrending method. These events are also the most unambiguous, and with the exception of 2006 these years can further be defined as extreme positive IOD events where the DMI exceeds +3σ for at least 1 month in the July–December interval. Other possible positive IOD events in 1982, 1991, 2008, 2012, and 2015 are less consistently classified, in that their determination as "events" is dependent upon methodological choices. As noted in the eastern and western SST time series (Fig. 3), the classification of 1982 and 2015 as positive IOD event years in some studies may be a false classification arising from a manifestation of El Niño-related warming in the western Indian Ocean (Stuecker et al., 2017; Zhao and Nigam, 2014).

This updated examination of IOD variability in high-quality observational records since 1981 has a number of important implications for the use of palaeoclimate evidence in assessing IOD variability. First, SST-based palaeoclimate studies located in the eastern IOD upwelling regions are likely to retain a stronger, more spatially stable, and less ambiguous signal of IOD variability than sites located in the western or central Indian Ocean. Second, the spatial pattern of rainfall anomalies associated with IOD variability appears to be insensitive to the exact regions used to define the IOD, suggesting that there is potential to reliably use proxy records from teleconnected regions to reconstruct past IOD impacts. Third, the seasonal constraints on IOD variability are an important consideration for palaeoclimate reconstructions of the IOD. For highly-resolved records, such as corals (bimonthly or higher resolution), isolating signals from the IOD-active season has the potential to improve the fidelity of IOD reconstructions. Signals of IOD variability may not be fully captured by proxies that only record signals during a particular season (e.g. summer climate signals preserved in tree growth), while for proxies that reconstruct past SST variance (such as individual foraminiferal analyses), the use of both mean-annual and seasonally-weighted specimens might provide a better view of interannual IOD variability. Finally, the method-dependent sensitivity of IOD event detection may mean that proxy evaluation of IOD variability in the past is most reliable for extreme positive IOD events that have an unambiguous signal, or better approached using an integrated measure of changes in proxy variability (e.g. moving standard deviation) and mean state instead of event detection approaches alone.

## 3. Palaeoclimate perspectives: trends in IOD variability and mean state

The recent IPCC special report on the Ocean and Cryosphere in a Changing Climate (SROCC) concluded that extreme positive IOD events are expected to occur more frequently in the 21st Century compared with the 20th Century (Collins et al., 2019; IPCC, 2019), but this assessment was assigned *low confidence* as it was based primarily on a single study (Cai et al., 2014) and may be an artifact of biases in the mean state and IOD variability within models (Li et al., 2016; Zheng et al., 2013). Bearing model biases in mind, projections across subsets of models from Phase 5 of the Coupled Model Intercomparison Project (CMIP5) that have reasonable representations of the IOD (Cai and Cowan, 2013; Cai et al., 2014, 2018) indicate that global warming during the 21st Century could accelerate warming of the western Indian Ocean and shoal the thermocline in the east, promoting a future mean climate state in the Indian Ocean that is more conducive to the development of positive IOD events (Cai et al., 2013, Cai et al., 2014). Limiting global warming to the 1.5 °C ambition of the Paris Agreement could result in the stabilisation of extreme positive IOD event frequency at double that of pre-industrial times (Cai et al., 2018), while unabated warming during the 21st Century could result in a tripling of the frequency of extreme positive IOD events this century compared to last (Cai et al., 2014). Palaeoclimate evidence provides insights into changes in IOD variability and mean state during the 20th Century and in pre-industrial times that gives perspective to these model-based projections of future IOD change.

A coral based reconstruction of the DMI has been produced back to the mid-19th Century (Abram et al., 2008), based on monthly and bi-monthly resolved oxygen isotope ($\delta^{18}O$) records from corals in the western and eastern tropical Indian Ocean (Abram et al., 2008; Charles et al., 1997, 2003; Pfeiffer and Dullo, 2006). Coral $\delta^{18}O$ reflects both the temperature of the seawater that the *Porites* corals grew in (with samples generally collected from less than 10 m water depth), as well as changes in the isotopic composition of seawater that are largely related to hydrological processes (Evans et al., 2000; Konecky et al., 2019; Lough, 2004; Thompson et al., 2011; Tierney et al., 2015a; Weber and Woodhead, 1972). The coral-based DMI can thus be considered as an integrated measure of coupled ocean–atmosphere variability of the IOD, capturing signals of warmer and wetter conditions in the west, and cooler and drier conditions in the east during positive IOD events (Abram et al., 2008). The detrended coral DMI demonstrates a significant increase in both the frequency and intensity of positive IOD events since the 1960s (Abram et al., 2008), a finding that was supported by a subsequent coral reconstruction from Kenya (Nakamura et al., 2009). Positive events occurred on average every 20 years at the start of the 20th Century, increasing to a recurrence interval of only 4 years by the end of the 20th Century (Abram et al., 2008).

An extended coral $\delta^{18}O$ reconstruction of IOD events during the last millennium from the eastern upwelling region further extends this perspective (Abram et al., 2020). The discontinuous, monthly-resolved reconstruction allows IOD variability to be examined across 500 years over the interval spanning 1240 to 2019 (representing 64% temporal coverage). This reconstruction highlights a mid-millennium shift in IOD variability at around 1590, which saw a tripling of positive IOD events from a mean recurrence time of once every 25 years prior to 1590, to once every 8 years from 1590 onwards (Abram et al., 2020). This mid-millennium shift in IOD variability is also seen in an intensification of ENSO variability at the same time (Rustic et al., 2015) (Section 5). Of the ten extreme positive IOD events detected since 1240 (Abram et al., 2020), four have occurred since 1960, and three since 1994, indicating that extreme positive IOD events have indeed become unusually

**Fig. 4. Variants of IOD indices and their spatial correlations with SST and rainfall.** (a) IOD indices based on the traditional West–East DMI (black), a Central–East variant (grey) and inverted anomalies only in the eastern DMI sector (blue) from OISSTv2 data (Reynolds et al., 2002). All data detrended by filtering to remove variability longer than 7 years (Saji et al., 1999). Horizontal lines indicate ±1.5σ variability based on a 1981–2010 climatological reference interval for each IOD index, and triangles (coloured to match the respective IOD index) indicate detection of a positive IOD event when that index exceeds +1.5σ for at least 2 months in July–December. Grey shading indicate positive IOD events detected across at least one of the three indices, with the addition of 1982 which is widely described as a positive IOD event (Abram et al., 2015) but may be influenced by spurious edge effects during detrending of the indices. (b–g) Spatial correlations of July–December means in SST (left; Reynolds et al., 2002) and rainfall (right; Adler et al., 2018) with the three variants of IOD indices shown in (a). Black boxes on SST panels show the regions used for defining the respective IOD indices.

frequent in the late 20th Century compared with the extended context of natural variability during the last millennium. The last millennium palaeoclimate data do not document any back-to-back positive IOD events (Abram et al., 2020). However, analysis of detrended instrumental data (Fig. 4a) also does not detect the 2006–2007–2008 sequential positive IOD events that some studies have discussed using non-detrended data (Cai et al., 2009b, 2009c), suggesting that detection of these events was linked to ongoing warming trends in the tropical Indian Ocean rather than true consecutive positive IOD events.

The combined coral and instrumental evidence for IOD variability and positive IOD event recurrence during the last millennium (Abram et al., 2020) is shown in Fig. 5 alongside output from the historical (1860–2005) and high greenhouse gas emissions Representative Concentration Pathway 8.5 (RCP8.5; 2006–2100) simulations from CMIP5 (Supplementary Table 1). There is a wide spread of future IOD trends across the 35-member multi-model ensemble. However, the multi-model means of the detrended DMI and detrended anomalies in just the eastern DMI region both suggest that positive and extreme positive IOD events become more frequent during the 21st Century under a high greenhouse gas emission scenario, while negative IOD events become less frequent (Fig. 5b–d). These trends become stronger when using only a subset of models assessed as having reliable representations of Indian Ocean climate variability (Cai et al., 2018). The context given by the last millennium data suggests that the pre-industrial range of positive and extreme positive IOD event numbers is similar to the range of variability across the historical simulation ensemble. Increases in positive and extreme positive IOD event frequency in recent decades are unusual in the context of variability in the last millennium, and will imminently move outside of the range of pre-industrial variability if these trends continue in line with the trends in RCP8.5 simulations (Fig. 5b and c).

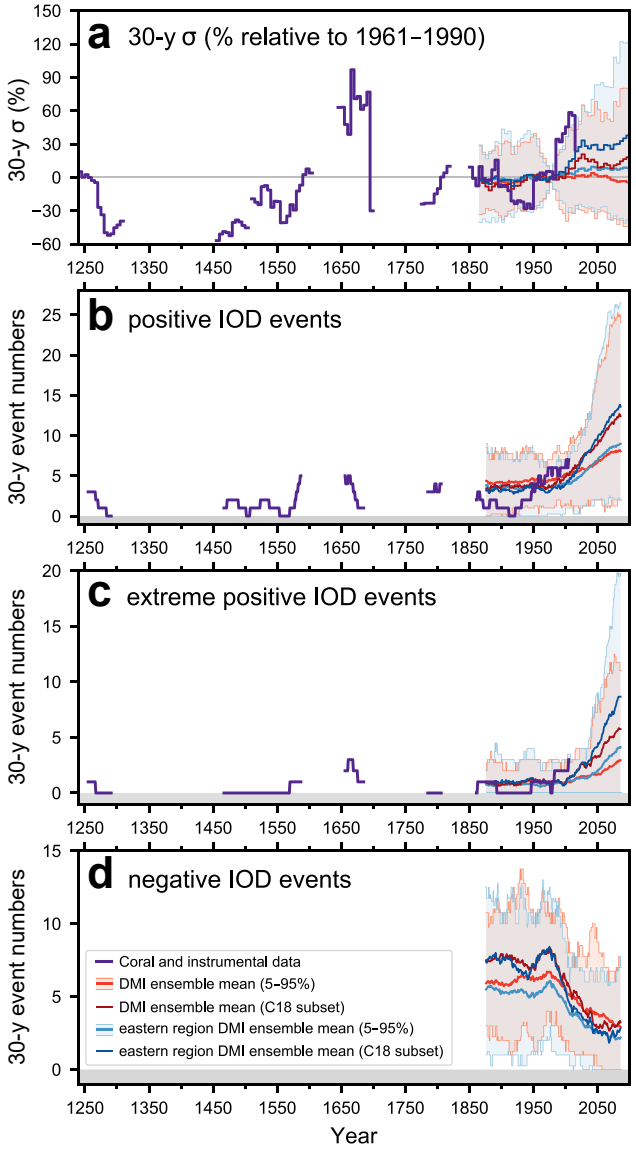


**Fig. 5. Past, recent and future IOD variability and event frequency.** Data are shown for coral and instrumental IOD data (Abram et al., 2020), and for a 35-member ensemble of CMIP5 historical and RCP8.5 simulations (Supplementary Table 1). A 12-member subset of CMIP5 simulations (C18) is based on model screening in (Cai et al., 2018). All data calculated relative to a 1961–1990 climatological reference interval and detrended to remove variability longer than 7-years before calculating IOD variability and events.

Trends in overall IOD-season variability are less consistent across the various lines of evidence (Fig. 5a). The current high level of July–December variability is not unprecedented in the context of the last millennium (and specifically the 17th Century), and the range of variability indicated by the coral data is larger than indicated by historical simulations of the CMIP5 ensemble (Fig. 5a). Similarly, the CMIP5 ensemble does not show a clear trend in IOD variability during the 21st Century, and while a positive trend emerges in the CMIP5 subset, it is characterised by a strong imprint of multi-decadal variability. The lack of a clear trajectory in overall IOD variability (Fig. 5a), despite strong and consistent recent and future trends in positive IOD event frequency (Fig. 5b–c), may be due to the tight coupling of tropical Indian Ocean variability to Pacific variability (Abram et al., 2020) (Section 5).

Recent and future increases in positive IOD event frequency have been linked in observations and model simulations to changes in the tropical ocean mean state, with the western Indian Ocean warming more rapidly than the eastern Indian Ocean (Gopika et al., 2019; Roxy et al., 2014), resulting in weakening of the zonal SST gradient and shoaling of the thermocline in the eastern equatorial Indian Ocean (Cai et al., 2008, Cai et al., 2009b). Observational SST data demonstrates this behaviour over recent decades (Table 1, Fig. 6a and b). Since 1981, the western DMI region has warmed at a rate of 0.12 °C per decade with similar rates of warming in January–June and July–December. Warming of the eastern DMI region has occurred at about half the rate of western warming (0.06 °C decade$^{-1}$), and is further suppressed when examining only the July–December interval (0.04 °C decade$^{-1}$). Extended SST products and CMIP5 models suggest that amplified warming of the western tropical Indian Ocean has been a characteristic of the full 20th Century (Roxy et al., 2014).

Reconstructed SST from a network of Indian Ocean coral records demonstrates that sustained and significant warming of the tropical Indian Ocean began in the mid-19th Century (Tierney et al., 2015a) (Fig. 6e). This onset of warming is consistent with a rapid response to early industrial-era greenhouse gas emissions, and was likely also accentuated by recovery from strong cooling in the early 19th Century related to large volcanic eruptions (Abram et al., 2016). Coral data from the western Indian Ocean has been used to independently verify historical SST data showing that the western Indian Ocean has warmed faster than any other tropical ocean region during the 20th Century (Pfeiffer et al., 2017). Trends in individual coral $\delta^{18}O$ records from the eastern and western DMI regions have also been used to suggest that the rate of warming since 1900 in the eastern region during the IOD season was suppressed relative to warming in months with no IOD influence, and

**Table 1**
**Observed regional SST trends.** SST linear trends with standard error are shown for the key IOD regions used in Fig. 4 using OISSTv2 since November 1981 (Reynolds et al., 2002).

| Region | Trend (°C per decade), all months | Trend (°C per decade), January–June averages | Trend (°C per decade), July–December averages |
|---|---|---|---|
| Western region (50°E–70°E, 10°S–10°N) | 0.12 ± 0.01 | 0.11 ± 0.04 | 0.12 ± 0.03 |
| Central region (60°E–90°E, 30°S–10°S) | 0.17 ± 0.01 | 0.15 ± 0.04 | 0.19 ± 0.04 |
| Eastern region (90°E–110°E, 10°S –equator) | 0.06 ± 0.02 | 0.07 ± 0.05 | 0.04 ± 0.06 |

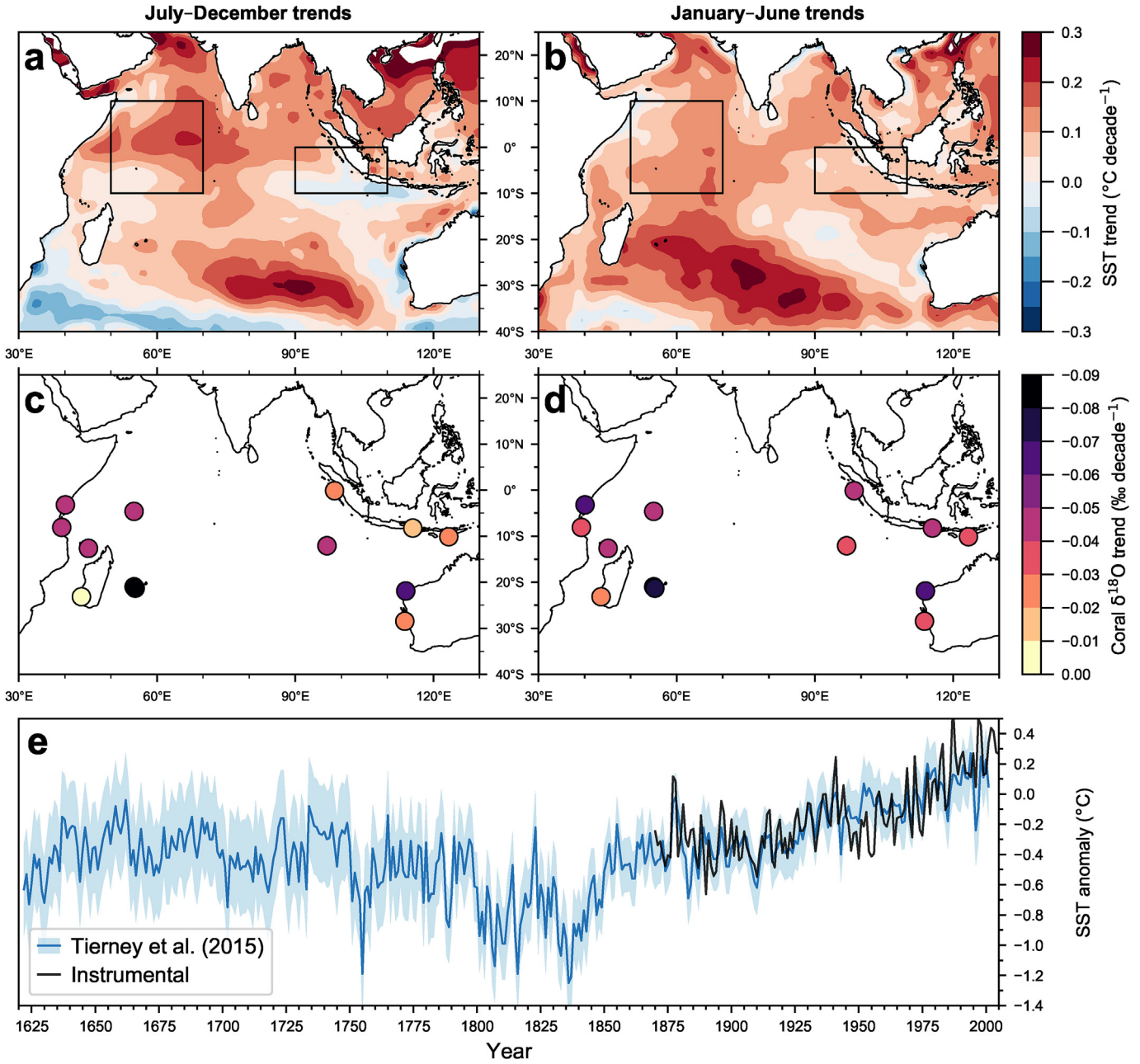


**Fig. 6. Trends in Indian Ocean** climate**.** Trends in (a–b) observed SST from OISSTv2 since November 1981 (Reynolds et al., 2002), and (c–d) coral $\delta^{18}O$ since 1900, calculated for (a–c) July–December and (b–d) January–June means. Negative trends in coral $\delta^{18}O$ (upwards direction on colour bar in c–d) represent changes toward warmer SST. Corals used in this analysis met the selection criteria of having bi-monthly or higher resolution, and covering more than 80 years of the 20th Century (Abram et al., 2008; Cahyarini et al., 2014; Charles et al., 1997, 2003; Damassa et al., 2006; Hennekam et al., 2018; Kuhnert et al., 1999, 2000; Nakamura et al., 2009; Pfeiffer et al., 2004, 2019; Zinke et al., 2004, 2008). Further details provided in Supplementary Table 2. (e) Tropical Indian Ocean SST anomaly (relative to 1961–1990) reconstruction for the Indian Ocean region spanning 15°S–20°N, 40°E–100°E (Tierney et al., 2015a). Thick blue line shows the "best" reconstruction based on reconstruction statistics and shading shows the root mean square error. Black curve shows HadISST instrumental data for the reconstruction target region.

relative to warming of the western region (Abram et al., 2008). An observed 20th Century strengthening of the southeasterly trade winds in the eastern Indian Ocean was proposed as a mechanism involved in suppression of eastern warming during the IOD-active season by causing intensified seasonal upwelling along the Java-Sumatra coast (Abram et al., 2008).

Using the network of Indian Ocean coral records compiled in the Ocean2k project (Tierney et al., 2015a), along with additional coral records published since this time, we expand upon previous studies to examine the spatial and temporal patterns of coral $\delta^{18}O$ trends in the tropical Indian Ocean during the 20th Century (Fig. 6c and d; see citation information for data sources in figure caption and Supplementary Table 2). The tropical Indian Ocean coral network demonstrates negative $\delta^{18}O$ trends indicative of a transition to a warmer and wetter mean state. Although the coral network is still relatively sparse it suggests that trends in the western Indian Ocean were stronger than in the equatorial eastern Indian Ocean, and were weaker in the IOD upwelling region of the equatorial eastern Indian Ocean in July–December compared with January–June trends (Supplementary Table 2). Thus, it appears that the spatial and seasonal characteristics of Indian Ocean SST trends observed since 1981 (Table 1) are representative of long-term climate trends across the full 20th Century. These sustained trends further highlight the importance of detrending observational, model and palaeoclimate data when examining interannual IOD variability in order to effectively distinguish between changes in interannual IOD variability and mean climate trends.

In summary, palaeoclimate data provide strong evidence that the IOD is undergoing changes that are unusual in the context of preindustrial times. Through the 20th Century the Indian Ocean has experienced: (i) an increase in the occurrence and intensity of positive IOD events, and (ii) a mean shift towards a more positive IOD-like mean state linked to amplified warming of the western equatorial Indian Ocean and suppressed warming of the eastern equatorial Indian Ocean that is most pronounced in the July–December half year. The palaeoclimate perspective provides an independent verification of changes detected in climate models run with anthropogenic greenhouse gas forcing, and the increasing frequency of positive IOD events will imminently move outside of the range of last millennium variability if projected trends continue.

## 4. Palaeoclimate perspectives: range of IOD variability

The IOD was formally defined 20 years ago following the extreme positive IOD event of 1997. This event remains the strongest ever recorded in detrended instrumental data,[1] and had widespread impacts on people and ecosystems. But it is unclear from short observational records if the extreme positive IOD event in 1997 is the strongest manifestation of positive IOD events that is possible. The possibility that the tropical Indian Ocean could harbour even stronger variability is of particular concern given CMIP5 projections of an increase in the frequency of extreme positive IOD events with ongoing climate warming (Fig. 5; Cai et al., 2014). Studies of ENSO variability in models suggest that many centuries of data are required to characterise the full range of unforced variability in the climate system (Stevenson et al., 2010; Wittenberg, 2009). This is further supported by the large range of interannual variability in pre-industrial coral records from the central Pacific (Cobb et al., 2013; Grothe et al., 2019). Palaeoclimate evidence from a range of different background climate states can be used to give context to the magnitude of recent IOD variability and the possibility that the instrumental record may not sample the full range of potential IOD states.

Observations, modelling and palaeoclimate evidence all point towards an increase in the frequency and strength of positive IOD events caused by anthropogenic climate warming (Section 3; Fig. 5). However, at least one eastern upwelling event even larger than the 1997 extreme positive IOD occurred prior to anthropogenic climate warming during the last millennium; estimated to have taken place in 1675. The July–December mean of this event was around 40% stronger than the 1997 event in coral $\delta^{18}O$ anomalies (Abram et al., 2020). This unusually large event appears to have occurred naturally in the absence of external forcing from a volcanic eruption (Sigl et al., 2015) or any historical evidence of a coincident extreme El Niño event (Gergis and Fowler, 2009; Grove and Adamson, 2018), both of which are proposed to play a role in promoting positive IOD events (Behera et al., 2006; Fischer et al., 2005; Maher et al., 2015). The moving 30-year variability of the IOD was also higher during much of the 17th Century than the high variability observed during recent decades, and this result holds even if the magnitude of the extreme 1675 event is capped at the level of the 1997 event (Abram et al., 2020).

Positive IOD events that were substantially stronger than the 1997 event have also been reconstructed from coral $\delta^{18}O$ and Sr/Ca (a proxy for SST) for the mid-Holocene at around 4400 years ago (Abram et al., 2003, 2007). The largest of these events had a peak cooling anomaly of 5.8 °C, around 50% larger than the peak cooling associated with the 1997 event in the northern Mentawai Islands (Abram et al., 2003). The mid-Holocene is a time when palaeoclimate records indicate that ENSO variability was reduced (Grothe et al., 2019; Thompson et al., 2017). At the same time the Asian summer monsoon was strengthened (Wang et al., 2005) and the Intertropical Convergence Zone (ITCZ) was located further north (Haug et al., 2001), representing a different background climate state to today. These broad-scale changes in Earth's climate variability are believed to have resulted from the altered amplitude of the seasonal cycle in insolation (Abram et al., 2007; Emile-Geay et al., 2016; Liu et al., 2014; Zinke et al., 2014), in conjunction with other factors such as a more vegetated Sahara (Pausata et al., 2017). Together the coral data on individual positive IOD events provides evidence that although the recent strengthening of positive IOD events is unusual, the magnitude of events that have been observed in recent decades are not outside of the range experienced prior to anthropogenic climate change.

Substantially stronger variability in the eastern IOD upwelling region is also reconstructed for the Last Glacial Maximum (LGM; 21,000 to 19,000 years ago; Fig. 7) (Thirumalai et al., 2019). Individual foram $\delta^{18}O$ analysis (IFA-$\delta^{18}O$) from a series of marine sediment cores along the Sumatran coast indicate that variability of upper-ocean mixed-layer temperatures under glacial conditions increased dramatically (up to 95% larger standard deviation relative to the late Holocene) (Fig. 7b–d). This increased variability appears to have occurred at both seasonal and interannual time scales. The spatial location of the seasonal component of these changes was focused on the southeastern Indian Ocean, characteristic of present day IOD variability. The equatorial sites also display an interannual component of enhanced variability during the LGM (Thirumalai et al., 2019). Based on assessment alongside simulations under LGM boundary conditions (including land-ocean configuration changes caused by lower sea level) (DiNezio et al., 2018), it has been proposed that intensified climate variability in the Indian Ocean during the LGM may have involved the emergence of an equatorial mode of variability that is not currently observed in the modern day system, and which involved dynamics similar to the modern El Niño in the Pacific (Thirumalai et al., 2019). The simulations indicate that the equatorial mode existed alongside the IOD with both having unique precursors, drivers, and different spatiotemporal patterns. Regardless, the simulations, supported by the IFA-$\delta^{18}O$, indicate that IOD variability was strengthened during the LGM (Fig. 7b–d).

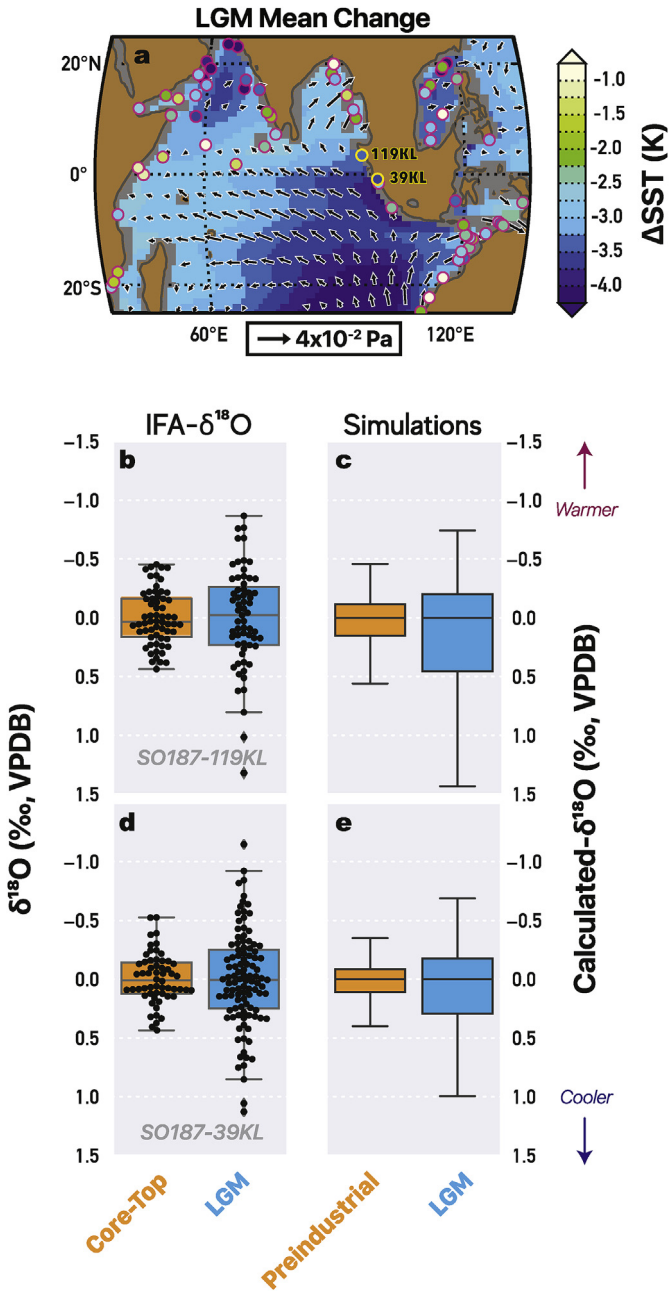


**Fig. 7. Changes in LGM mean state and variability in the Indian Ocean.** (a) Model-data comparison between proxy reconstructions of SST (circles) and simulated changes with CESM1.2 (filled colour) under LGM conditions in the tropical Indian Ocean (DiNezio et al., 2018). Changes in wind stress (arrows) from the model simulation are also depicted and two eastern equatorial Indian Ocean core sites are highlighted in yellow whose IFA-$\delta^{118}$O data are shown below. (b, d) Reconstructed IFA-$\delta^{18}$O variability at the LGM for (b) Core Site SO187-119 KL (3.52°N, 96.32°E) and for (d) Core Site SO187-39 KL (0.3°S, 99.9°E) along with corresponding (c, e) simulated changes in calculated-$\delta^{18}$O variability at the core locations' gridpoints. $\delta^{18}$O values were calculated using SST and SSS fields from the model (see Thirumalai et al., 2019, for details). Median values (and thus, LGM cooling) were removed for both reconstructed data and the simulated output.

In each of these past times of elevated IOD variability and extreme positive IOD events, there is additional palaeoclimate evidence that suggests mean SST conditions were cooler than present in the eastern Indian Ocean and that the East-to-West SST gradient across the basin was reduced. These mean state changes indicate that enhanced IOD variability in the past was associated with a more positive IOD-like mean SST configuration across the equatorial Indian Ocean.

During the last 2000 years, the Indo-Pacific Warm Pool (IPWP) experienced cool and variable SSTs during the Little Ice Age (Oppo et al., 2009). Cool conditions peaked at around 1700, when SSTs in Makassar Strait were around 0.5–1 °C cooler than present day (Oppo et al., 2009). At the same time, marine sediment cores from the Gulf of Aden in the western equatorial Indian Ocean indicate that the zonal SST gradient reached a minimum (Tierney et al., 2010) such that there was effectively no mean East-to-West gradient across the equatorial Indian Ocean (see Section 6 for further discussion).

Similarly for the mid-Holocene, a large compilation of coral mean SST estimates indicates that waters along the coast of Sumatra were 1.2 °C ± 0.3 °C cooler than present between 5500 and 4300 years ago (years before present, where present is 1950) (Abram et al., 2009). This was hypothesised to be related to a northward movement or contraction of the IPWP due to a strengthened Asian summer monsoon and a northerly shift in the ITCZ at this time (Abram et al., 2009; Griffiths et al., 2010a). Mid-Holocene SST cooling is also reconstructed in a near-decadal resolution marine sediment core from the Mentawai basin (Mohtadi et al., 2014), however analysis of lower resolution marine sediment cores from along the Sumatran coast show less coherent Holocene SST patterns (Li et al., 2018). A marine sediment core from offshore Tanzania demonstrates that basin-wide cooling across the tropical Indian Ocean characterised the mid-Holocene interval. This western Indian Ocean marine sediment core indicates that SST was 0.47 °C ± 0.27 °C cooler than present day between 5600 and 4200 years ago, and that the thermocline was deeper than today (Kuhnert et al., 2014). This basin-wide SST cooling may represent a situation where cooling was greater in the east than the west, and thus resulted in a mean positive IOD-like mean state in the Indian Ocean. Warm and wet anomalies over eastern Africa (Gasse, 2000; Thompson et al., 2002), and cool and dry anomalies over southern Indonesia (Griffiths et al., 2010a, 2010b), provide additional evidence of a positive IOD-like mean response of the atmosphere during this mid-Holocene interval.

Marine sediment core evidence for changes in mean SST in the Indian Ocean is clearer for the LGM (Fig. 7a). The network of palaeoclimate data indicate strong cooling in the eastern Indian Ocean, contrasting with more mild cooling in the western Indian Ocean and implying a reduction in the mean zonal SST gradient relative to preindustrial times (DiNezio et al., 2018; Thirumalai et al., 2019). Overall cooling is reflective of global scale SST cooling associated with the last ice age, but enhanced cooling in the eastern Indian Ocean is geographically controlled by exposure of the Sunda and Sahul shelves, which restricted the Indonesian throughflow and altered atmospheric convection patterns over the maritime continent (DiNezio and Tierney, 2013; DiNezio et al., 2018). Modelling of SST anomalies with modern day climate forcing but a closed Indonesian throughflow similarly produce cooler SSTs in the eastern Indian Ocean and a drastically transformed mode of tropical variability that bears a close resemblance to El Niño-type dynamics (Kajtar et al., 2015).

Overall, the palaeoclimate data provide compelling evidence that the tropical Indian Ocean can harbour stronger variability than that which has been observed during the instrumental era. It also strengthens the evidence that changes in variability of the IOD are closely coupled to changes in the mean zonal SST gradient across the tropical Indian Ocean. Past intervals with elevated IOD variability (e.g. 17th Century, mid-Holocene and Last Glacial Maximum) also saw enhanced cooling in the eastern region and reduction/reversal of the zonal SST gradient indicative of a more positive IOD-like mean state. Human-caused climate warming is also now

causing a shift to a more positive IOD-like mean state (Section 3), although in this case because the western Indian Ocean is warming faster than the eastern Indian Ocean. The palaeoclimate evidence for past positive IOD-like mean states with larger interannual IOD variability than observed in recent decades has important implications for future climate risk management associated with IOD impacts, particularly in the context of the multiple lines of evidence for an increasing frequency and intensity of positive IOD events underway now.

## 5. Palaeoclimate perspectives: coupling of IOD variability to the tropical Pacific

One of the most contentious aspects of IOD research has been the interdependence of the IOD with ENSO. The range of perspectives extend from the IOD being an independent climate mode (Saji et al., 1999; Webster et al., 1999) that is able to induce super El Niño events in the Pacific Ocean (Hameed et al., 2018), through to the IOD being solely the manifestation of ENSO variability into the Indian Ocean combined with stochastic noise (Stuecker et al., 2017). The original paper defining the DMI described the IOD as an independent mode that had a weak ($r < 0.35$) correlation with SST anomalies in the NINO3 region, and noted the occurrence of significant positive IOD events during El Niño, La Niña and neutral ENSO phases (Saji et al., 1999). Other subsequent studies of the IOD–ENSO relationship have concluded that the atmosphere and ocean anomalies associated with El Niño events can precondition the Indian Ocean to be more conducive to the development of positive IOD events (Behera et al., 2006; Fischer et al., 2005; Wang, 2019). Decadal to multi-decadal scale variability in the Pacific Ocean can also promote the occurrence of positive IOD events by altering subsurface heat content in the eastern Indian Ocean via the Indonesian Throughflow (Ummenhofer et al., 2017), and can modulate the strength of the interannual IOD–ENSO relationship through time (Lim et al., 2017). Other studies have contended that variability in the regions used to define the IOD is not independent of ENSO, and that the IOD feature reported in the literature should be considered an integral part of ENSO evolution (Allan et al., 2001; Stuecker et al., 2017; Zhao and Nigam, 2014). Recent developments have seen a shift towards a more integrated approach in describing tropical climate variability that involves interactions between each of the three tropical ocean basins (Cai et al., 2019; Wang, 2019), including two-way interactions between the IOD and ENSO (Wang et al., 2019).

A serious limitation in resolving our understanding of IOD–ENSO relationships is the lack of long, high-quality instrumental data for the tropical Indian and Pacific oceans. Our updated seasonal analysis of Indian Ocean SST patterns using high quality data from 1981 to 2019 suggests that the July–December EOF1 is strongly correlated with El Niño events (Fig. 2), and that there is potential for false positive IOD events to be characterised by the DMI when strong ENSO-related warming occurs in the western Indian Ocean in the absence of a coupled eastern Indian Ocean IOD response (Fig. 3; Fig. 4). Extended SST products since the mid 19th-Century are available (Rayner et al., 2003; Smith et al., 2008), but include known biases (Pfeiffer et al., 2017), and do not adequately capture the signal of SST cooling during positive IOD events in the eastern Indian Ocean (Fig. 3a). Furthermore, the use of these products to examine IOD–ENSO relationships is problematic as infilling methods for data sparse times and regions invoke present day teleconnection patterns. This infilling has the potential to artificially bias the IOD–ENSO relationship in poorly observed parts of these products to replicate the relationships in well-observed recent decades. Palaeoclimate data provide an independent means to overcome these limitations and provide a long-term view on the IOD–ENSO relationship.

Precisely dated coral records can be used to examine long-term relationships of interannual variability between the tropical Indian and Pacific Oceans. Coral records from multiple sites in the western Indian Ocean demonstrate the strong imprint of ENSO teleconnections into this region (Charles et al., 1997; Damassa et al., 2006; Pfeiffer and Dullo, 2006; Pfeiffer et al., 2004; Zinke et al., 2004, 2005), consistent with analysis of observational data (Zhao and Nigam, 2014) including the EOF analysis presented in Fig. 2. The coral records demonstrate that the imprint of ENSO variability into the western Indian Ocean has persisted across multiple centuries (Damassa et al., 2006; Zinke et al., 2004), and includes interannual and decadal timescales of variability (Ault et al., 2009). Signals in the western equatorial Indian Ocean appear to have a stable teleconnection to ENSO (Charles et al., 1997; Pfeiffer and Dullo, 2006), whereas this relationship is non-stationary in the central equatorial Indian Ocean and only evident in the south-western Indian Ocean at times when ENSO variability is strong (Zinke et al., 2005).

Coral records from the eastern Indian Ocean provide insights into IOD–ENSO interactions during the last millennium. The coral DMI since 1846 (Abram et al., 2008) demonstrates that there is temporal variability in the strength of the IOD–ENSO correlation. IOD–ENSO correlations were weak between 1905 and 1960, coinciding with an interval of reduced ENSO variance and suggesting that IOD–ENSO interactions are strongest when ENSO variability itself is strong (Abram et al., 2008). Coral data from the eastern IOD upwelling region during the last millennium build upon this finding by demonstrating a persistent, tight coupling between the magnitude of IOD and ENSO variance (Abram et al., 2020). During the last millennium there was around 45% shared variance in the magnitude of interannual variability between the IOD and ENSO, such that intervals of reduced (strengthened) IOD variance co-occurred with intervals of reduced (strengthened) ENSO variance (Abram et al., 2020; see also Fig. 9 in Section 6).

Changes in the mean state of the Pacific Ocean were associated with broad-scale patterns of changing ENSO–IOD variance. In particular, the first half of the last millennium was characterised by a La Niña-like mean state in the equatorial Pacific SST gradient (enhanced West–East gradient), and an approximately 30% reduction in the magnitude of IOD and ENSO interannual variance (relative to 1961–1990 climatology) (Abram et al., 2020; Rustic et al., 2015). A mid-millennium shift at around 1590 saw a transition to a more El Niño-like mean state in the equatorial Pacific SST gradient (reduced West–East gradient) and an increase in IOD and ENSO interannual variance to levels similar to present day. This included an interval during the 17th Century where IOD and ENSO variance were higher than in recent decades and the mean SST gradient across the equatorial Pacific also reached its most diminished level of the last millennium (Abram et al., 2020; Rustic et al., 2015; see also Section 6).

The persistent association of IOD and ENSO variance does not necessarily imply that all positive IOD events are associated with an El Niño event in the Pacific. A direct comparison of the timing of individual IOD and ENSO events between palaeoclimate records is confounded by even very small uncertainties in the absolute age of fossil coral material. However, the characteristic seasonal progression of SST anomalies in the eastern IOD upwelling region during co-occurring positive IOD and El Niño events (Figs. 2 and 3a) provides a way to test event-level associations in the palaeoclimate

[1] Note: The magnitude of the 2019 extreme positive IOD event exceeded the 1997 event in non-detrended data due to the strong anthropogenic warming signal and shift towards a more positive IOD-like mean state in the tropical Indian Ocean.

record without any age uncertainty.

Here, we use recently published coral data from the southern Mentawai Islands (Abram et al., 2020) to identify positive IOD events in July–December data and basin-wide warming associated with El Niño events in January–June data. A modern coral $\delta^{18}O$ record (Fig. 8a) demonstrates robust detection of cool/dry anomalies associated with positive IOD events known from instrumental data. Most El Niño events known from the instrumental SST record are also detected as warm/wet anomalies in January–June in the same coral record indicating potential to use these anomalies as an indication of IOBM warming in the eastern Indian Ocean that is likely associated with El Niño activity. Across the last millennium coral data (Fig. 8b–d), this same event detection method identifies 21 positive IOD events that occurred without subsequent warming indicative of the IOBM, and 12 positive IOD events followed by warming that may be indicative of a co-occurring El Niño event. There are a further 55 warm events detected in the coral data that are not preceded by a positive IOD event, although composite analysis indicates that in some cases positive IOD events may occur in the July–December interval following a January–June warming event. There are limitations in this analysis in how confidently El Niño events can be prescribed to all January–June warming events in the eastern IOD region, however the coral data clearly shows that there are frequent examples from the palaeoclimate record of positive IOD events occurring without any indication of an accompanying El Niño event. The composites also suggest that there is a tendency for positive IOD events that co-occur with El Niño events to be stronger than their positive IOD-only counterparts. This extended view provided by the last millennium coral data strengthens conclusions from the observational record; El Niño events in the Pacific can promote the development of positive IOD events, however ultimately positive IOD events can develop with or without co-occurring El Niño events in the Pacific Ocean.

The coupling of IOD–ENSO variance reconstructed during the last millennium appears to have not persisted in very different climate states. For example, strengthened IOD upwelling and cooler

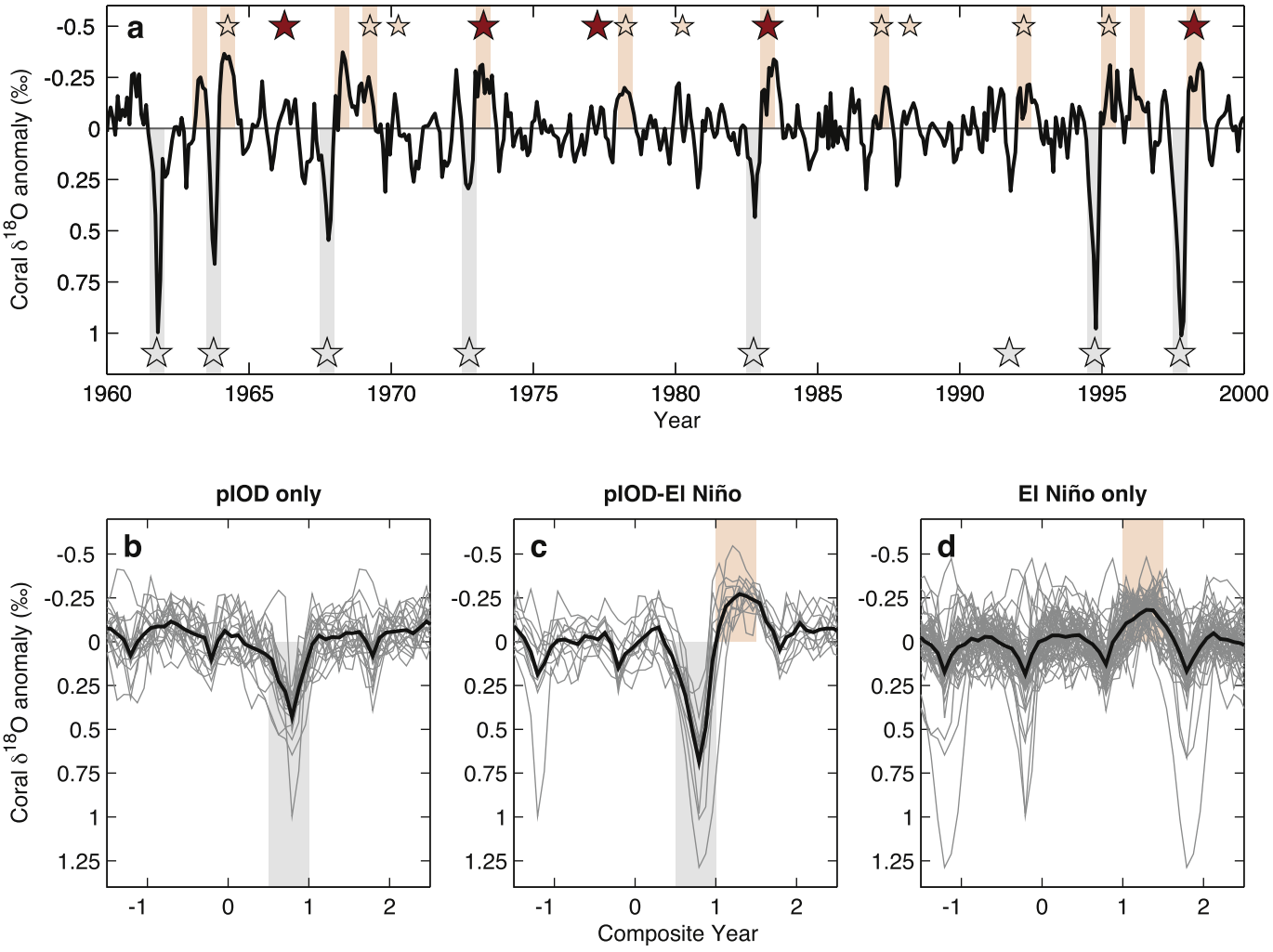


**Fig. 8. Seasonal coral $\delta^{18}O$ anomalies in the eastern Indian Ocean during the last millennium.** Coral $\delta^{18}O$ anomalies from the southern Mentawai Islands were detrended by removing variability longer than 7 years, and anomalies in July–December were used to detect positive IOD events (grey shading) relative to 1961–1990 variability following the methods of Abram et al. (2020). Warm/wet anomalies in January–June where the 3-month smoothed coral $\delta^{18}O$ anomaly data exceeded $-1\sigma$ for at least 2 months are used as indicative markers of El Niño-related basin wide warming (orange shading). (a) Event detection in a modern coral $\delta^{18}O$ anomaly record (black curve) relative to positive IOD events detected in observational SST data (grey stars; Fig. 4; Abram et al., 2015), and central Pacific (small orange stars) and eastern Pacific (large red stars) type El Niño events (Freund et al., 2019; Ren and Jin, 2011). (b–c) Composites from the last millennium coral data for (b) independent positive IOD events (n = 21), for (c) positive IOD events followed by warm anomalies indicative of a co-occurring El Niño event (n = 12), and for (d) warm events indicative of El Niño events in the absence of a positive IOD event in the previous July–December interval (n = 55). Composites are aligned so detected positive IOD events occur in July–December of year 0 and warm anomalies indicative of El Niño events occur in January–June of year 1. Thin grey lines show coral $\delta^{18}O$ anomalies of individual sequences and thick black curves show composite mean across individual sequences.

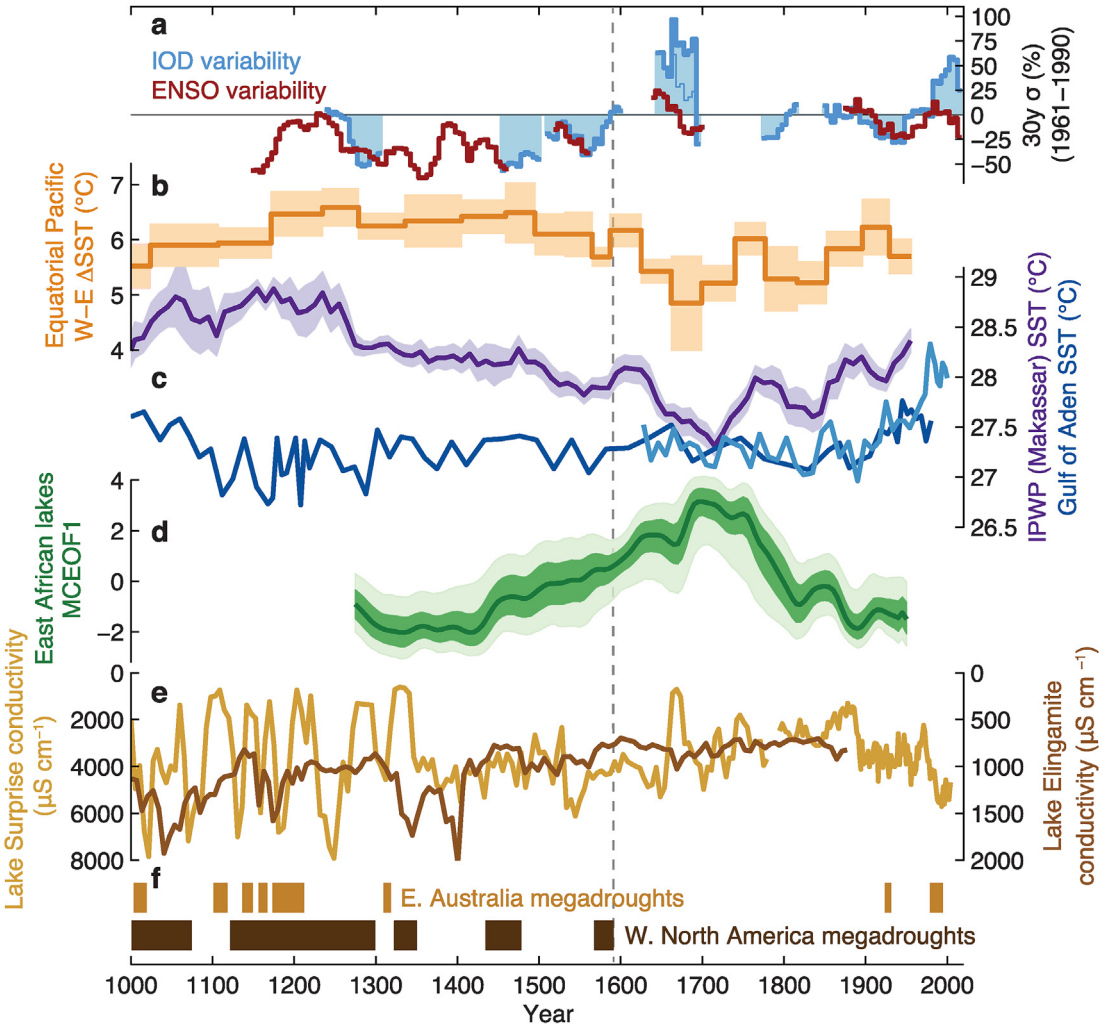
a
IOD variability
ENSO variability
30y σ (%) (1961–1990)
b
Equatorial Pacific W–E ΔSST (°C)
c
IPWP (Makassar) SST (°C)
Gulf of Aden SST (°C)
d
East African lakes MCEOF1
e
Lake Surprise conductivity (µS cm⁻¹)
Lake Elingamite conductivity (µS cm⁻¹)
f
E. Australia megadroughts
W. North America megadroughts
Year

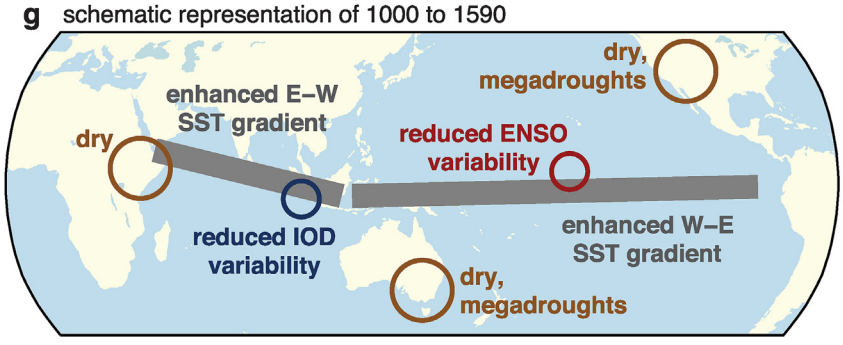
g schematic representation of 1000 to 1590
dry, megadroughts
enhanced E–W SST gradient
dry
reduced ENSO variability
reduced IOD variability
enhanced W–E SST gradient
dry, megadroughts

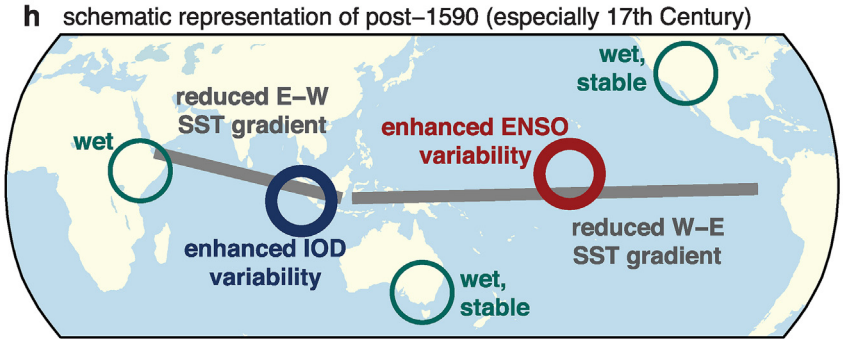
h schematic representation of post–1590 (especially 17th Century)
wet, stable
reduced E–W SST gradient
wet
enhanced ENSO variability
enhanced IOD variability
reduced W–E SST gradient
wet, stable

mean SST in the eastern DMI region during the mid-Holocene (Abram et al., 2007, 2009) (Section 4) coincided with a time when palaeoclimate evidence indicate a significant reduction in ENSO variance (Emile-Geay et al., 2016; Grothe et al., 2019). Although a matter of debate, palaeoclimate data and model evidence points to diminished ENSO variance during the LGM (Ford et al., 2015; Zhu et al., 2017), whereas available evidence from the Indian Ocean suggest heightened variability linked to a stronger IOD and the emergence of an equatorial mode (Fig. 7; Thirumalai et al., 2019). Thus it appears that ENSO and the IOD need not be coupled in their overall characteristics under dramatically different mean climates.

In summary, the palaeoclimate evidence supports the emerging view that IOD and ENSO variability can be seen in the framework of pan-tropical climate interactions, rather than either of the extreme views of the IOD being entirely independent of ENSO or entirely a manifestation of ENSO variability. In the climate conditions of the last millennium and present day there is a tight coupling between the magnitude of interannual variability of the IOD and ENSO, but on an individual event level positive IOD events have commonly occurred without any indication of a co-occurring El Niño event. This IOD–ENSO interaction does not appear to persist under very different mean climate states in the past, such as the LGM and mid-Holocene, which raises questions about whether today's IOD–ENSO interactions could change in a rapidly warming future climate.

## 6. Palaeoclimate perspectives: impacts of IOD variability on regional hydroclimate

The IOD has a strong impact on regional hydroclimate patterns and extremes. For example, observational data indicate that the worst droughts in southeast Australia during the 20th Century were associated with an absence of negative IOD states that deprived the region of its normal (Austral) winter and spring moisture (Ashok et al., 2003; Cai et al., 2009b; Ummenhofer et al., 2009). During positive IOD events, the lower rainfall and higher temperatures in southeastern Australia precondition the region for significant bushfires in the following summer, and could be a more important factor in increasing regional bushfire risk than El Niño events (Cai et al., 2009a). Accurate simulations of future climate change impacts, including from IOD variability, are an essential aspect of climate risk reduction through improved seasonal forecasting as well as societal adaptation and resilience building. However, at least some aspects of recent and future IOD impacts appear to be poorly represented in current climate models. For example, in the Horn of Africa region (equatorial east Africa), climate simulations indicate a wetting trend that is at odds with observed drying in recent decades (Tierney et al., 2015; Ummenhofer et al., 2018). This is related to over estimation of the September–November "short rains" in model simulations that is caused, in some cases, by an overly strong simulated IOD (Tierney et al., 2015).

Palaeoclimate evidence can help to identify the regional risks associated with changing IOD variability, and to identify spurious aspects of simulated impacts. However, it is important to first take note of potential limitations in the use of palaeoclimate records to infer the impacts of past climate variability. In most cases the impacts reconstructed with palaeoclimate records are a teleconnected response within the climate system, and their interpretation relies on an assumption that the spatial patterns of these teleconnected responses has remained stable through time. This may not always be a valid assumption: reconstructions of ENSO variability over the last millennium that are based on teleconnected signals produce inconsistent data (Dätwyler et al., 2019) at times when ENSO variability was weak (Abram et al., 2020). The IOD is also known to be inconsistently represented in precipitation-related proxies due to the changing strength of the IOD-precipitation relationship, and over the last millennium the spatial signature of reliable IOD impact signals may be restricted to only multi-decadal to multi-centennial timescales (Konecky et al., 2014). A further consideration is that in many locations rainfall impacts are the combination of multiple aspects of climate variability. For example, rainfall in southeastern Australia is strongly influenced by the IOD, along with ENSO and the Southern Annular Mode (SAM) (Risbey et al., 2009). When regional impacts are modulated by multiple—at times co-varying—climate drivers, attribution of reconstructed changes to a specific climate process or mode is challenging and requires that data is interpreted in a broad framework (Fig. 9).

Hydroclimate reconstructions for eastern Africa during the last millennium are available from a network of lake basins, including records of charcoal, run-off, lake level and leaf wax isotopes (Tierney et al., 2013). Analysis of the shared climate signals across this network over the last 700 years identifies a spatial structure of anomalies that resemble the pattern of IOD-related anomalies across this region. The network of hydroclimate indicators suggests that dry conditions prevailed over the Horn of Africa until around 1400 followed by a transition to wetter conditions that peaked at around 1700 (Tierney et al., 2013) (Fig. 9d). A leaf wax isotope record from the Gulf of Aden (not shown in Fig. 9) further indicates that the 17th Century was the wettest period of the last 2000 years in equatorial East Africa (Tierney et al., 2015). Pronounced drying during the 20th Century in this region is unusual rapid in the context of the last 2000 years, may have an anthropogenic component, and in instrumental records is associated with a decline in the March–May "long rains" rather than an IOD-related trend (Tierney et al., 2015).

The evolution of east African rainfall during the last millennium (Fig. 9d) closely matches SST changes in the Indonesian Throughflow region of Makassar Strait (Fig. 9c), with peak cooling in the Indo-Pacific Warm Pool (and presumably also the eastern Indian Ocean) coinciding with the 17th Century maximum in rainfall over the Horn of Africa (Oppo et al., 2009; Tierney et al., 2013). SST reconstructed from Gulf of Aden marine sediment cores (Tierney et al., 2015) shows an antiphase relationship to the Makassar Strait record (Fig. 9c), indicative of IOD-like zonal modulation of Indian Ocean SST. In particular, the records from these sites show that the East to West SST gradient was reduced to near zero during the 17th Century. The palaeoclimate evidence is consistent with strengthened Walker circulation across the Indian Ocean during the

**Fig. 9. Hydroclimate impacts during the last millennium**. Reconstructions of oceanic IOD–ENSO variability from (a) coral records of the moving 30-year variability in 5-year time steps for the IOD (blue) and ENSO (red), expressed as percent change relative to 1961–1990 (Abram et al., 2020; Cobb et al., 2003, 2013; Dee et al., 2020; Grothe et al., 2019). Thin blue line shows IOD variability where the magnitude of the extreme 1675 event is capped at the magnitude of the 1997 event (Abram et al., 2020). SST reconstructions are shown for (b) marine sediment core records of the mean SST gradient between the western and eastern equatorial Pacific (Rustic et al., 2015), along with (c) SST from within the IPWP (Oppo et al., 2009) and from the Gulf of Aden in the western equatorial Indian Ocean (Tierney et al., 2015). Reconstructions of hydroclimate impacts for (d) a network of east African lakes based showing the Monte Carlo EOF1 of shared variability (Tierney et al., 2013), (e) diatom-inferred conductivity in two lakes from southeast Australia (Barr et al., 2014), and (f) reconstructed intervals of megadrought in eastern Australia (Vance et al., 2015) and western North America (Cook et al., 2016). Hydroclimate timeseries (d, e) are orientated such that upward anomalies reflect increased effective moisture in the key IOD impact areas of equatorial east Africa and southeast Australia. (g, h) Schematic representations of the data in a-f for intervals of the last millennium (g) before and (h) after the ~1590 mid-millennium shift (dashed vertical line in panels a–f).

early part of the last millennium that transitioned to maximum weakening of the Walker circulation by the 17th Century (Tierney et al., 2013). ENSO variability is an important driver of Indian Ocean Walker circulation strength on annual to interannual timescales, however observations and unforced ocean–atmosphere model simulations indicate that on timescales longer than 10 years it is instead the zonal gradient in the equatorial Indian Ocean SST that is the primary influence on the strength of the Walker circulation across the Indian Ocean and the associated impacts on East African rainfall (Tierney et al., 2013; Ummenhofer et al., 2018).

Hydroclimate reconstructions from the Indonesian region are available in high resolution for the last millennium from marine and lake sediments (Konecky et al., 2013; Oppo et al., 2009; Tierney et al., 2010) and speleothems (Griffiths et al., 2016). This is a region where multiple climate drivers interact, complicating the interpretation of the palaeorecords. Palaeoclimate records from this region have frequently been interpreted as indicators of long-term ENSO changes (Griffiths et al., 2016), however hydroclimate indicators produce ENSO histories for the last millennium that are at odds with ocean-based reconstructions of the ENSO mean state and variability (Rustic et al., 2015; Yan et al., 2015). Similarly, interpretation of these signals in terms of North-South migration of ITCZ associated with changes in the strength of the Asian summer monsoon (Tierney et al., 2010) has been challenged by new data from the Australian monsoon region (Denniston et al., 2016). Instead, it appears that in the IPWP region during the last millennium changes in hydroclimate reflect intervals of expansion and contraction of the latitudinal width of the tropical rainfall belt (Denniston et al., 2016; Yan et al., 2015). During the 17th Century the tropical rainfall belt experienced its most extreme contraction of the last millennium (Denniston et al., 2016) and hydroclimate records from the central region of the IPWP documented extreme wet conditions (Griffiths et al., 2016; Tierney et al., 2010) despite cooler mean SST in the region (Oppo et al., 2009). In this context, and with the distribution of currently available hydroclimate records, it is not possible to assess how last millennium changes in the IOD may have also impacted rainfall in the Indonesian region.

In southeastern Australia, lake sediments provide a history of effective moisture (precipitation minus evaporation) in the region through the last millennium until European settlement (Barr et al., 2014; Tyler et al., 2015). The interval from 1400 to 1880 experienced high effective moisture and low interdecadal variability (Barr et al., 2014). In contrast, 850–1400 was characterised by a drier mean climate, with large multidecadal swings in lake hydrology (Barr et al., 2014; Fig. 9e). Strong multi-decadal variability in east Australian rainfall is also inferred indirectly from the Law Dome ice core record, which indicates a prevalence of megadroughts prior to 1400 including an unprecedented century of aridity over the 12th Century (Vance et al., 2015; Fig. 9f). Western North America also experienced clustering of unusually frequent megadroughts in the first half of the last millennium, prior to a transition to a wetter mean climate state around the mid-millennium (Ault et al., 2018; Cook et al., 2016; Fig. 9f). Both of these characteristics of western North American hydroclimate change are unable to be explained by internal, unforced variability (Ault et al., 2018). Last Millennium simulations indicate that clustering of frequent western North American megadroughts during the first half of the last millennium may instead be the result of frequent cold ENSO anomalies (La Niña conditions) in the tropical Pacific Ocean (Coats et al., 2013, 2016).

A coherent picture emerges across the Indo-Pacific that prior to the mid-millennium shift in IOD and ENSO variability and mean state (Abram et al., 2020; Fig. 9a–c; Section 5), regional hydroclimate regimes included a drier mean climate with stronger multidecadal variability and more frequent megadroughts in equatorial east Africa, southeastern Australian and western North America (Fig. 9d–f). Conversely, conditions after the mid-millennium involved a wetter mean state with increased influence of interannual variability in all of these regions. These coherent changes across all three regions can not be explained through mean-state changes replicating the spatial patterns of interannual IOD and ENSO impacts (i.e. if this were the case then southeastern Australia would be expected to be wet when western North America and/or equatorial East Africa were dry, and vice versa).

The mean hydroclimate changes reconstructed during the last millennium may instead be explained through changes in the strength of interannual IOD and ENSO variability (Fig. 9a).[2] Natural variability experiments have shown that droughts in atmosphere-only models can last longer than in models that also include ocean variability (Taschetto et al., 2016). This is because interannual ENSO (and IOD) variability acts as a terminating mechanism for wet and dry events. In the case of southeastern Australia, La Niña or negative IOD events are crucial for bringing the widespread, heavy rainfall that breaks otherwise dry conditions (King et al., 2020; Ummenhofer et al., 2009). Strengthened interannual IOD and ENSO variability after ~1590 (Abram et al., 2020) may thus have promoted a more stable mean hydroclimate regime across the Indo-Pacific by providing stronger and more frequent occurrences of the IOD-ENSO conditions needed to bring rainfall and prevent prolonged dry spells. Conversely, reduced interannual IOD and ENSO variability prior to ~1590 could account for the frequent and prolonged droughts on both sides of the Pacific basin, while also allowing Indian Ocean SSTs to play a stronger role in controlling Walker circulation and east African rainfall. Schematics summarising these Indo-Pacific climate states and impacts are presented for the 1000 to 1590 interval including transitional conditions in some impacts from around 1400 (Fig. 9g), and for the post 1590 interval with peak conditions experienced around the 17th Century (Fig. 9h).

Overall, the palaeoclimate archive points toward the importance of interannual IOD and ENSO variability in breaking droughts. This strengthens observational evidence that recent droughts in southeastern Australia were characterised by an absence of negative IOD events (Ummenhofer et al., 2009), and suggests that increased IOD and ENSO variability results in a wetter and more stable mean hydroclimate regime across the Indo-Pacific. It also cautions that the impacts of multi-decadal climate variability and mean state changes may not simply result in a more persistent manifestation of the spatial hydroclimate anomalies associated with interannual IOD and ENSO variability.

## 7. Conclusions

This review has demonstrated the many insights that palaeoclimate evidence has to offer in understanding IOD variability, and the context that this gives to recent and future trajectories of change. A summary of these insights includes:

***IOD trends***. Palaeoclimate data provide strong evidence that the trends in recent decades towards more frequent and more intense positive IOD events are unusual in the context of preindustrial times. This transition has coincided with a mean shift towards a more positive IOD-like mean state linked to amplified warming of the western equatorial Indian Ocean and suppressed warming of the eastern equatorial Indian Ocean that is most pronounced in the

[2] We note that changes during the last millennium in the strength and variability of the Southern Annular Mode would have also impacted the hydroclimate of southeastern Australia, and that changes in SAM may also have covaried with ENSO changes. A thorough assessment of any SAM influence is beyond the scope of this review.

July–December half year. The palaeoclimate perspective provides an independent verification of changes detected in climate models run with anthropogenic greenhouse gas forcing, and demonstrates that the increasing frequency of positive IOD events will imminently move outside of the range of last millennium variability if projected trends continue.

***IOD variability***. Palaeoclimate data demonstrate that the tropical Indian Ocean can harbour stronger variability than that which has been observed during the instrumental era. The magnitude of IOD variability in the past has been closely coupled to changes in the mean zonal SST gradient across the tropical Indian Ocean. Past intervals with elevated interannual IOD variability (e.g. 17th Century, mid-Holocene, Last Glacial Maximum) also involved mean cooling in the eastern region and a reduction of the zonal SST gradient (due to stronger cooling in the east than the west), representing a more positive IOD-like mean state. The potential for even stronger IOD events than has been observed in the instrumental record has important implications for managing the future climate risks associated with IOD impacts, particularly when viewed in conjunction with the multiple lines of evidence for a currently increasing frequency and intensity of positive IOD events.

***IOD–ENSO interactions***. The palaeoclimate evidence supports viewing IOD and ENSO variability in a framework of pan-tropical climate interactions, rather than the IOD being entirely independent of ENSO or entirely a manifestation of ENSO variability. Through the last millennium there has been a tight coupling between the magnitude of interannual variability of the IOD and ENSO, but on an individual event level positive IOD events have commonly occurred without any indication of a co-occurring El Niño event. This IOD–ENSO interaction does not appear to persist under very different mean climate states in the past, which raises questions around how the coupling between these two tropical modes could change in a rapidly warming future climate.

***IOD impacts***. The palaeoclimate archive points to the importance of interannual IOD and ENSO variability in breaking droughts. Extended droughts in southeast Australia and the western U.S. and dry conditions in equatorial east Africa all coincided with reduced IOD–ENSO variability during the first half of the last millennium, while a wetter and more stable hydroclimate established across the Indo-Pacific when IOD–ENSO variability strengthened after the mid millennium. The palaeoclimate view of long-term hydroclimate changes cautions that the impacts of multi-decadal climate variability and mean state changes may not simply result in a more persistent manifestation of the spatial hydroclimate anomalies associated with interannual IOD and ENSO variability.

Overall, this review highlights the rich insights into the IOD that can be gained from palaeoclimate evidence. Palaeoclimate data helps to overcome known limitations in observations and model simulations of the IOD, and demonstrates that strong conclusions about the IOD and its impacts can be reached when the evidence for past, present and future behaviour of the IOD are viewed together.

## Declaration of competing interests

The authors declare that they have no known competing financial interests or personal relationships that could have appeared to influence the work reported in this paper.

## Acknowledgements

This work was supported by the Australian Research Council through the Centre of Excellence for Climate Extremes (CE170100023; NJA, JAH, NMW, CCU, MHE), and a Future Fellowship to NJA (FT160100029); JAH is supported by an Australian Research Training Program (RTP) scholarship; KT acknowledges National Science Foundation (NSF) grant OCE1903482 for support; CCU acknowledges support by NSF under AGS-1602455 and *The Andrew W. Mellon Foundation Endowed Fund for Innovative Research* at WHOI. MHE is also supported by the Earth Science and Climate Change Hub of the Australian Government's National Environmental Science Programme (NESP).

## Appendix A. Supplementary data

Supplementary data to this article can be found online at https://doi.org/10.1016/j.quascirev.2020.106302.

## References

Abram, N.J., Dixon, B.C., Rosevear, M.G., Plunkett, B., Gagan, M.K., Hantoro, W.S., Phipps, S.J., 2015. Optimized coral reconstructions of the Indian Ocean Dipole: an assessment of location and length considerations. Paleoceanography 30, 1391–1405.

Abram, N.J., Gagan, M.K., Cole, J.E., Hantoro, W.S., Mudelsee, M., 2008. Recent intensification of tropical climate variability in the Indian Ocean. Nat. Geosci. 1, 849–853. https://doi.org/10.1038/ngeo357.

Abram, N.J., Gagan, M.K., Liu, Z.Y., Hantoro, W.S., McCulloch, M.T., Suwargadi, B.W., 2007. Seasonal characteristics of the Indian Ocean Dipole during the Holocene epoch. Nature 445, 299–302. https://doi.org/10.1038/nature05477.

Abram, N.J., Gagan, M.K., McCulloch, M.T., Chappell, J., Hantoro, W.S., 2003. Coral reef death during the 1997 Indian Ocean dipole linked to Indonesian wildfires. Science 301, 952–955.

Abram, N.J., McGregor, H.V., Gagan, M.G., Hantoro, W.S., Suwargadi, B.W., 2009. Changes in the southern extent of the Indo-Pacific Warm Pool during the mid-Holocene. Quat. Sci. Rev. 28, 2794–2803. https://doi.org/10.1016/j.quascirev.2009.07.006.

Abram, N.J., McGregor, H.V., Tierney, J.E., Evans, M.N., McKay, N.P., Kaufman, D.S., Thirumalai, K., Martrat, B., Goosse, H., Phipps, S.J., Steig, E.J., Kilbourne, K.H., Saenger, C.P., Zinke, J., Leduc, G., Addison, J.A., Mortyn, P.G., Seidenkrantz, M.-S., Sicre, M.-A., Selvaraj, K., Filipsson, H.L., Neukom, R., Gergis, J., Curran, M.A.J., Gunten, L.v., 2016. Early onset of industrial-era warming across the oceans and continents. Nature 536, 411–418. https://doi.org/10.1038/nature19082.

Abram, N.J., Wright, N.M., Ellis, B., Dixon, B.C., Wurtzel, J.B., England, M.H., Ummenhofer, C.C., Philibosian, B., Cahyarini, S.Y., Yu, T.-L., Shen, C.-C., Cheng, H., Edwards, L.A., Heslop, D., 2020. Coupling of Indo-Pacific climate variability over the last millennium. Nature 579, 385–392. https://doi.org/10.1038/s41586-020-2084-4.

Adler, R., Sapiano, M., Huffman, G., Wang, J.-J., Gu, G., Bolvin, D., Chiu, L., Schneider, U., Becker, A., Nelkin, E., Xie, P., Ferraro, R., Shin, D.-B., 2018. The global precipitation climatology project (GPCP) monthly analysis (new version 2.3) and a review of 2017 global precipitation. Atmosphere 9, 138. https://doi.org/10.3390/atmos9040138.

Allan, R., Chambers, D., Drosdowsky, W., Hendon, H.H., Latif, M., Nicholls, N., Smith, I., Stone, R., Tourre, Y., 2001. Is there an Indian Ocean Dipole, and is it independent of the El Niño - Southern Oscillation. CLIVAR Exchanges 6, 18–22.

Anderson, W.B., Seager, R., Baethgen, W., Cane, M., You, L., 2019. Synchronous crop failures and climate-forced production variability. Sci. Adv. 5, eaaw1976.

Anonymous, 1994. Indian Ocean may have El Niño of its own. Eos. Trans. Am. Geophys. Union 75, 585–586.

Ashok, K., Guan, Z., Yamagata, T., 2003. Influence of the Indian Ocean Dipole on the Australian winter rainfall. Geophys. Res. Lett. 30 https://doi.org/10.1029/2003GL017926.

Ault, T.R., Cole, J.E., Evans, M.N., Barnett, H., Abram, N.J., Tudhope, A.W., Linsley, B.K., 2009. Intensified decadal variability in tropical climate during the late 19th century. Geophys. Res. Lett. 36 https://doi.org/10.1029/2008GL036924.

Ault, T.R., George, S.S., Smerdon, J.E., Coats, S., Mankin, J.S., Carrillo, C.M., Cook, B.I., Stevenson, S., 2018. A robust null hypothesis for the potential causes of megadrought in western North America. J. Clim. 31, 3–24.

Banzon, V., Smith, T.M., Chin, T.M., Liu, C., Hankins, W., 2016. A long-term record of blended satellite and in situ sea-surface temperature for climate monitoring, modeling and environmental studies. Earth Syst. Sci. Data 8, 165–176.

Barr, C., Tibby, J., Gell, P., Tyler, J., Zawadzki, A., Jacobsen, G.E., 2014. Climate variability in south-eastern Australia over the last 1500 years inferred from the high-resolution diatom records of two crater lakes. Quat. Sci. Rev. 95, 115–131.

Behera, S.K., Luo, J.J., Masson, S., Rao, S.A., Sakuma, H., Yamagata, T., 2006. A CGCM study on the interaction between IOD and ENSO. J. Clim. 19, 1688–1705.

Behera, S.K., Yamagata, T., 2001. Subtropical SST dipole events in the southern Indian Ocean. Geophys. Res. Lett. 28, 327–330.

Bellenger, H., Guilyardi, E., Leloup, J., Lengaigne, M., Vialard, J., 2014. ENSO representation in climate models: from CMIP3 to CMIP5. Clim. Dynam. 42, 1999–2018.

Birkett, C., Murtugudde, R., Allan, T., 1999. Indian Ocean climate event brings floods to east Africa's lakes and the sudd marsh. Geophys. Res. Lett. 26, 1031–1034.

Brown, J.R., Moise, A.F., Colman, R., Zhang, H., 2016. Will a warmer world mean a wetter or drier Australian monsoon? J. Clim. 29, 4577–4596.

Cahyarini, S.Y., Pfeiffer, M., Nurhati, I.S., Aldrian, E., Dullo, W.-C., Hetzinger, S., 2014. Twentieth century sea surface temperature and salinity variations at Timor inferred from paired coral $\delta^{18}O$ and Sr/Ca measurements. J. Geophys. Res.: Oceans 119, 4593–4604.

Cai, W., Borlace, S., Lengaigne, M., van Rensch, P., Collins, M., Vecchi, G., Timmermann, A., Santoso, A., McPhaden, M.J., Wu, L., England, M.H., Wang, G., Guilyardi, E., Jin, F.-F., 2014b. Increasing frequency of extreme El Niño events due to greenhouse warming. Nat. Clim. Change 4, 111–116.

Cai, W., Cowan, T., 2013. Why is the amplitude of the Indian Ocean Dipole overly large in CMIP3 and CMIP5 climate models? Geophys. Res. Lett. 40, 1200–1205.

Cai, W., Cowan, T., Raupach, M., 2009a. Positive Indian Ocean Dipole events precondition southeast Australia bushfires. Geophys. Res. Lett. 36 https://doi.org/10.1029/2009GL039902.

Cai, W., Cowan, T., Sullivan, A., 2009b. Recent unprecedented skewness towards positive Indian Ocean Dipole occurrences and its impact on Australian rainfall. Geophys. Res. Lett. 36 https://doi.org/10.1029/2009GL037604.

Cai, W., Qiu, Y., 2012. An observation-based assessment of nonlinear feedback processes associated with the Indian Ocean Dipole. J. Clim. 26, 2880–2890.

Cai, W., Santoso, A., Wang, G., Weller, E., Wu, L., Ashok, K., Masumoto, Y., Yamagata, T., 2014a. Increased frequency of extreme Indian Ocean Dipole events due to greenhouse warming. Nature 510, 254–258.

Cai, W., Sullivan, A., Cowan, T., 2008. Shoaling of the off-equatorial south Indian Ocean thermocline: is it driven by anthropogenic forcing? Geophys. Res. Lett. 35 https://doi.org/10.1029/2008GL034174.

Cai, W., Sullivan, A., Cowan, T., 2009c. Climate change contributes to more frequent consecutive positive Indian Ocean Dipole events. Geophys. Res. Lett. 36, L23704.

Cai, W., Wang, G., Gan, B., Wu, L., Santoso, A., Lin, X., Chen, Z., Jia, F., Yamagata, T., 2018. Stabilised frequency of extreme positive Indian Ocean Dipole under 1.5 °C warming. Nat. Commun. 9, 1419.

Cai, W., Wu, L., Lengaigne, M., Li, T., McGregor, S., Kug, J.-S., Yu, J.-Y., Stuecker, M.F., Santoso, A., Li, X., Ham, Y.-G., Chikamoto, Y., Ng, B., McPhaden, M.J., Du, Y., Dommenget, D., Jia, F., Kajtar, J.B., Keenlyside, N., Lin, X., Luo, J.-J., Martín-Rey, M., Ruprich-Robert, Y., Wang, G., Xie, S.-P., Yang, Y., Kang, S.M., Choi, J.-Y., Gan, B., Kim, G.-I., Kim, C.-E., Kim, S., Kim, J.-H., Chang, P., 2019. Pantropical climate interactions. Science 363, eaav4236.

Cai, W., Zheng, X.-T., Weller, E., Collins, M., Cowan, T., Lengaigne, M., Yu, W., Yamagata, T., 2013. Projected response of the Indian Ocean Dipole to greenhouse warming. Nat. Geosci. 6, 999–1007.

Chan, D., Kent, E.C., Berry, D.I., Huybers, P., 2019. Correcting datasets leads to more homogeneous early-twentieth-century sea surface warming. Nature 571, 393–397.

Charles, C.D., Cobb, K.M., Moore, M.D., Fairbanks, R.G., 2003. Monsoon-tropical ocean interaction in a network of coral records spanning the 20th century. Mar. Geol. 201, 207–222.

Charles, C.D., Hunter, D.E., Fairbanks, R.G., 1997. Interaction between the ENSO and the asian monsoon in a coral record of tropical climate. Science 277, 925–928.

Coats, S., Smerdon, J.E., Cook, B.I., Seager, R., 2013. Stationarity of the tropical pacific teleconnection to North America in CMIP5/PMIP3 model simulations. Geophys. Res. Lett. 40, 4927–4932.

Coats, S., Smerdon, J.E., Cook, B.I., Seager, R., Cook, E.R., Anchukaitis, K.J., 2016. Internal ocean-atmosphere variability drives megadroughts in Western North America. Geophys. Res. Lett. 43, 9886–9894.

Cobb, K.M., Charles, C.D., Cheng, H., Edwards, R.L., 2003. El Niño/Southern Oscillation and tropical Pacific climate during the last millennium. Nature 424, 271–276.

Cobb, K.M., Westphal, N., Sayani, H.R., Watson, J.T., Di Lorenzo, E., Cheng, H., Edwards, R.L., Charles, C.D., 2013. Highly variable El Niño/Southern Oscillation throughout the Holocene. Science 339, 67–70.

Collins, M., Sutherland, M., Bouwer, L., Cheong, S.-M., Frölicher, T., Combes, H.J.D., Roxy, M.K., Losada, I., McInnes, K., Ratter, B., Rivera-Arriaga, E., Susanto, R.D., Swingedouw, D., Tibig, L., 2019. Extremes, abrupt changes and managing risk. In: Pörtner, H.-O., Roberts, D.C., Masson-Delmotte, V., Zhai, P., Tignor, M., Poloczanska, E., Mintenbeck, K., Alegría, A., Nicolai, M., Okem, A., Petzold, J., Rama, B., Weyer, N.M. (Eds.), IPCC Special Report on the Ocean and Cryosphere in a Changing Climate.

Cook, B.I., Cook, E.R., Smerdon, J.E., Seager, R., Williams, A.P., Coats, S., Stahle, D.W., Díaz, J.V., 2016. North American megadroughts in the Common Era: reconstructions and simulations. Wiley Interdiscip. Rev.: Clim. Change 7, 411–432.

Damassa, T.D., Cole, J.E., Barnett, H.R., Ault, T.R., McClanahan, T.R., 2006. Enhanced multidecadal climate variability in the seventeenth century from coral isotope records in the western Indian Ocean. Paleoceanography 21. https://doi.org/10.1029/2005PA001217.

Dätwyler, C., Abram, N.J., Grosjean, M., Wahl, E.R., Neukom, R., 2019. El Niño–Southern Oscillation variability, teleconnection changes and responses to large volcanic eruptions since AD 1000. Int. J. Climatol. 39, 2711–2724. https://doi.org/10.1002/joc.5983.

Dee, S.G., Cobb, K.M., Emile-Geay, J., Ault, T.R., Edwards, R.L., Cheng, H., Charles, C.D., 2020. No consistent ENSO response to volcanic forcing over the last millennium. Science 367, 1477–1481. https://doi.org/10.1126/science.aax2000.

Denniston, R.F., Ummenhofer, C.C., Wanamaker, A.D., Lachniet, M.S., Villarini, G., Asmerom, Y., Polyak, V.J., Passaro, K.J., Cugley, J., Woods, D., Humphreys, W.F., 2016. Expansion and contraction of the indo-pacific tropical rain belt over the last three millennia. Sci. Rep. 6, 34485.

DiNezio, P.N., Tierney, J.E., 2013. The effect of sea level on glacial Indo-Pacific climate. Nat. Geosci. 6, 485–491.

DiNezio, P.N., Tierney, J.E., Otto-Bliesner, B.L., Timmermann, A., Bhattacharya, T., Rosenbloom, N., Brady, E., 2018. Glacial changes in tropical climate amplified by the Indian Ocean. Sci. Adv. 4, eaat9658.

Emile-Geay, J., Cobb, K.M., Carré, M., Braconnot, P., Leloup, J., Zhou, Y., Harrison, S.P., Corrège, T., McGregor, H.V., Collins, M., Driscoll, R., Elliot, M., Schneider, B., Tudhope, A., 2016. Links between tropical Pacific seasonal, interannual and orbital variability during the Holocene. Nat. Geosci. 9, 168–173.

England, M.H., Ummenhofer, C.C., Santoso, A., 2006. Interannual rainfall extremes over southwest western Australia linked to Indian Ocean climate variability. J. Clim. 19, 1948–1969.

Epstein, P.R., 1999. Climate and health. Science 285, 347. https://doi.org/10.1126/science.285.5426.347.

Evans, M.N., Kaplan, A., Cane, M.A., 2000. Intercomparison of coral oxygen isotope data and historical sea surface temperature (SST): potential for coral-based SST field reconstructions. Paleoceanography 15, 551–563.

Feng, M., McPhaden, M.J., Xie, S.-P., Hafner, J., 2013. La Niña forces unprecedented Leeuwin Current warming in 2011. Sci. Rep. 3, 1277.

Fischer, A.S., Terray, P., Guilyardi, E., Gualdi, S., Delecluse, P., 2005. Two independent triggers for the Indian Ocean Dipole/zonal mode in a coupled GCM. J. Clim. 18, 3428–3449.

Ford, H.L., Ravelo, A.C., Polissar, P.J., 2015. Reduced El niño–southern oscillation during the last glacial maximum. Science 347, 255. https://doi.org/10.1126/science.1258437.

Freund, M.B., Henley, B.J., Karoly, D.J., McGregor, H.V., Abram, N.J., Dommenget, D., 2019. Higher frequency of Central Pacific El Nino events in recent decades relative to past centuries. Nat. Geosci. 12, 450–455.

Gasse, F., 2000. Hydrological changes in the african tropics since the last glacial maximum. Quat. Sci. Rev. 19, 189–211.

Gergis, J.L., Fowler, A.M., 2009. A history of ENSO events since A.D. 1525: implications for future climate change. Climatic Change 92, 343–387.

Gopika, S., Izumo, T., Vialard, J., Lengaigne, M., Suresh, I., Kumar, M.R.R., 2019. Aliasing of the Indian Ocean externally-forced warming spatial pattern by internal climate variability. Clim. Dynam. 54, 1093–1111. https://doi.org/10.1007/s00382-019-05049-9.

Griffiths, M.L., Drysdale, R.N., Gagan, M.K., Frisia, S., Zhao, J.-x., Ayliffe, L.K., Hantoro, W.S., Hellstrom, J.C., Fischer, M.J., Feng, Y.-X., Suwargadi, B.W., 2010a. Evidence for Holocene changes in Australian–Indonesian monsoon rainfall from stalagmite trace element and stable isotope ratios. Earth Planet Sci. Lett. 292, 27–38.

Griffiths, M.L., Drysdale, R.N., Vonhof, H.B., Gagan, M.K., Zhao, J.-x., Ayliffe, L.K., Hantoro, W.S., Hellstrom, J.C., Cartwright, I., Frisia, S., Suwargadi, B.W., 2010b. Younger Dryas–Holocene temperature and rainfall history of southern Indonesia from $\delta^{18}O$ in speleothem calcite and fluid inclusions. Earth Planet Sci. Lett. 295, 30–36.

Griffiths, M.L., Kimbrough, A.K., Gagan, M.K., Drysdale, R.N., Cole, J.E., Johnson, K.R., Zhao, J.-X., Cook, B.I., Hellstrom, J.C., Hantoro, W.S., 2016. Western Pacific hydroclimate linked to global climate variability over the past two millennia. Nat. Commun. 7, 11719.

Grothe, P.R., Cobb, K.M., Liguori, G., Di Lorenzo, E., Capotondi, A., Lu, Y., Cheng, H., Edwards, R.L., Southon, J.R., Santos, G.M., Deocampo, D.M., Lynch-Stieglitz, J., Chen, T., Sayani, H.R., Thompson, D.M., Conroy, J.L., Moore, A.L., Townsend, K., Hagos, M., O'Connor, G., Toth, L.T., 2019. Enhanced El Niño-Southern Oscillation variability in recent decades. Geophys. Res. Lett. 47 https://doi.org/10.1029/2019GL083906 e2019GL083906.

Grove, R., Adamson, G., 2018. El Niño chronology and the Little ice age. In: Grove, R., Adamson, G. (Eds.), El Niño in World History. Palgrave Macmillan UK, London, pp. 49–79.

Hameed, S.N., Jin, D., Thilakan, V., 2018. A model for super El Niños. Nat. Commun. 9, 2528.

Han, W., Vialard, J., McPhaden, M.J., Lee, T., Masumoto, Y., Feng, M., Ruijter, W.P.M.d., 2014. Indian ocean decadal variability: a review. Bull. Am. Meteorol. Soc. 95, 1679–1703.

Hashizume, M., Chaves, L.F., Minakawa, N., 2012. Indian Ocean Dipole drives malaria resurgence in East African highlands. Sci. Rep. 2, 269.

Hastenrath, S., Nicklis, A., Greischar, L., 1993. Atmospheric-hydrospheric mechanisms of climate anomalies in the western equatorial Indian Ocean. J. Geophys. Res.: Oceans 98, 20219–20235.

Haug, G.H., Hughen, K.A., Sigman, D.M., Peterson, L.C., Röhl, U., 2001. Southward migration of the intertropical convergence zone through the Holocene. Science 293, 1304. https://doi.org/10.1126/science.1059725.

Hennekam, R., Zinke, J., van Sebille, E., ten Have, M., Brummer, G.-J.A., Reichart, G.-J., 2018. Cocos (Keeling) corals reveal 200 Years of multidecadal modulation of southeast Indian ocean hydrology by Indonesian throughflow. Paleoceanogr. Paleoclimat. 33, 48–60.

IPCC, 2019. Summary for Policymakers. In: Pörtner, H.-O., Roberts, D.C., Masson-Delmotte, V., Zhai, P., Tignor, M., Poloczanska, E., Mintenbeck, K., Alegría, A., Nicolai, M., Okem, A., Petzold, J., Rama, B., Weyer, N.M. (Eds.), IPCC Special Report on the Ocean and Cryosphere in a Changing Climate. World Meteorological Organization.

Kajtar, J.B., Santoso, A., England, M.H., Cai, W., 2015. Indo-Pacific climate interactions in the absence of an Indonesian throughflow. J. Clim. 28, 5017–5029.

Kataoka, T., Tozuka, T., Behera, S., Yamagata, T., 2014. On the Ningaloo niño/niña. Clim. Dynam. 43, 1463–1482.

King, A.D., Pitman, A.J., Henley, B.J., Ukkola, A.M., Brown, J.R., 2020. The role of climate variability in Australian drought. Nat. Clim. Change 10, 177–179.

Konecky, B., Russell, J., Vuille, M., Rehfeld, K., 2014. The Indian Ocean Zonal Mode over the past millennium in observed and modeled precipitation isotopes. Quat. Sci. Rev. 103, 1–18.
Konecky, B.L., Noone, D.C., Cobb, K.M., 2019. The influence of competing hydroclimate processes on stable isotope ratios in tropical rainfall. Geophys. Res. Lett. 46, 1622–1633. https://doi.org/10.1029/2018GL080188.
Konecky, B.L., Russell, J.M., Rodysill, J.R., Vuille, M., Bijaksana, S., Huang, Y., 2013. Intensification of southwestern Indonesian rainfall over the past millennium. Geophys. Res. Lett. 40, 386–391.
Kuhnert, H., Kuhlmann, H., Mohtadi, M., Meggers, H., Baumann, K.-H., Pätzold, J., 2014. Holocene tropical western Indian Ocean sea surface temperatures in covariation with climatic changes in the Indonesian region. Paleoceanography 29, 423–437.
Kuhnert, H., Pätzold, J., Hatcher, B., Wyrwoll, K.H., Eisenhauer, A., Collins, L.B., Zhu, Z.R., Wefer, G., 1999. A 200-year coral stable oxygen isotope record from a high-latitude reef off Western Australia. Coral Reefs 18, 1–12.
Kuhnert, H., Pätzold, J., Wyrwoll, K.H., Wefer, G., 2000. Monitoring climate variability over the past 116 years in coral oxygen isotopes from Ningaloo Reef, Western Australia. Int. J. Earth Sci. 88, 725–732.
Li, G., Xie, S.-P., Du, Y., 2016. A robust but spurious pattern of climate change in model projections over the tropical Indian ocean. J. Clim. 29, 5589–5608.
Li, Z., Chen, M.-T., Lin, D.-C., Shi, X., Liu, S., Wang, H., Yokoyama, Y., Shen, C.-C., Mii, H.-S., Troa, R.A., Zuraida, R., Triarso, E., Hendrizan, M., 2018. Evidence of solar insolation and internal forcing of sea surface temperature changes in the eastern tropical Indian Ocean during the Holocene. Quat. Int. 490, 1–9.
Lim, E.-P., Hendon, H.H., 2017. Causes and predictability of the negative Indian Ocean Dipole and its impact on La Niña during 2016. Sci. Rep. 7, 12619.
Lim, E.-P., Hendon, H.H., Zhao, M., Yin, Y., 2017. Inter-decadal variations in the linkages between ENSO, the IOD and south-eastern Australian springtime rainfall in the past 30 years. Clim. Dynam. 49, 97–112.
Linthicum, K.J., Anyamba, A., Tucker, C.J., Kelley, P.W., Myers, M.F., Peters, C.J., 1999. Climate and satellite indicators to forecast rift valley fever epidemics in Kenya. Science 285, 397. https://doi.org/10.1126/science.285.5426.397.
Liu, Z., Lu, Z., Wen, X., Otto-Bliesner, B.L., Timmermann, A., Cobb, K.M., 2014. Evolution and forcing mechanisms of El Niño over the past 21,000 years. Nature 515, 550–553.
Lough, J.M., 2004. A strategy to improve the contribution of coral data to high-resolution paleoclimatology. Palaeogeogr. Palaeoclimatol. Palaeoecol. 204, 115–143.
Mach, K.J., Mastrandrea, M.D., Freeman, P.T., Field, C.B., 2017. Unleashing expert judgment in assessment. Global Environ. Change 44, 1–14.
Maher, N., McGregor, S., England, M.H., Gupta, A.S., 2015. Effects of volcanism on tropical variability. Geophys. Res. Lett. 42, 6024–6033.
Masson-Delmotte, V., Schulz, M., Abe-Ouchi, A., Beer, J., Ganopolski, A., Rouco, J.F.G., Jansen, E., Lambeck, K., Luterbacher, J., Naish, T., Osborn, T., Otto-Bliesner, B., Quinn, T., Ramesh, R., Rojas, M., Shao, X., Timmermann, A., 2013. Information from paleoclimate archives. In: Stocker, T.F., Qin, D., Plattner, G.-K., Tignor, M., Allen, S.K., Boschung, J., Nauels, A., Xia, Y., Bex, V., Midgley, P.M. (Eds.), Climate Change 2013: the Physical Science Basis. Contribution of Working Group I to the Fifth Assessment Report of the Intergovernmental Panel on Climate Change. Cambridge University Press, Cambridge, United Kingdom and New York, NY, USA.
Meyers, G., McIntosh, P., Pigot, L., Pook, M., 2007. The years of El Niño, La Niña, and interactions with the tropical Indian Ocean. J. Clim. 20, 2872–2880.
Mohtadi, M., Prange, M., Oppo, D.W., De Pol-Holz, R., Merkel, U., Zhang, X., Steinke, S., Lückge, A., 2014. North Atlantic forcing of tropical Indian Ocean climate. Nature 509, 76–80.
Morioka, Y., Tozuka, T., Yamagata, T., 2010. Climate variability in the southern Indian Ocean as revealed by self-organizing maps. Clim. Dynam. 35, 1059–1072.
Nakamura, N., Kayanne, H., Iijima, H., McClanahan, T.R., Behera, S.K., Yamagata, T., 2009. Mode shift in the Indian Ocean climate under global warming stress. Geophys. Res. Lett. 36 https://doi.org/10.1029/2009GL040590.
Nicholls, N., 1989. sea surface temperatures and Australian winter rainfall. J. Clim. 2, 965–973.
Oppo, D.W., Rosenthal, Y., Linsley, B.K., 2009. 2,000-year-long temperature and hydrology reconstructions from the Indo-Pacific warm pool. Nature 460, 1113–1116.
Pausata, F.S.R., Zhang, Q., Muschitiello, F., Lu, Z., Chafik, L., Niedermeyer, E.M., Stager, J.C., Cobb, K.M., Liu, Z., 2017. Greening of the Sahara suppressed ENSO activity during the mid-Holocene. Nat. Commun. 8, 16020.
Pfeiffer, M., Dullo, W.-C., 2006. Monsoon-induced cooling of the western equatorial Indian Ocean as recorded in coral oxygen isotope records from the Seychelles covering the period of 1840-1994AD. Quat. Sci. Rev. 25, 993–1009.
Pfeiffer, M., Dullo, W.-C., Eisenhauer, A., 2004. Variability of the intertropical convergence zone recorded in coral isotopic records from the central Indian Ocean (Chagos Archipelago). Quat. Res. 61, 245–255.
Pfeiffer, M., Reuning, L., Zinke, J., Garbe-Schönberg, D., Leupold, M., Dullo, W.-C., 2019. 20th century $\delta^{18}O$ seawater and salinity variations reconstructed from paired $\delta^{18}O$ and Sr/Ca measurements of a La Reunion coral. Paleoceanogr. Paleoclimat. 34, 2183–2200. https://doi.org/10.1029/2019PA003770.
Pfeiffer, M., Zinke, J., Dullo, W.C., Garbe-Schönberg, D., Latif, M., Weber, M.E., 2017. Indian Ocean corals reveal crucial role of World War II bias for twentieth century warming estimates. Sci. Rep. 7, 14434.
Rayner, N.A., Parker, D.E., Horton, E.B., Folland, C.K., Alexander, L.V., Rowell, D.P., Kent, E.C., Kaplan, A., 2003. Global analyses of sea surface temperature, sea ice, and night marine air temperature since the late nineteenth century. J. Geophys. Res. 108, 4407. https://doi.org/10.1029/2002jd002670.
Ren, H.-L., Jin, F.-F., 2011. Niño indices for two types of ENSO. Geophys. Res. Lett. 38 https://doi.org/10.1029/2010GL046031.
Reynolds, R.W., Rayner, N.A., Smith, T.M., Stokes, D.C., Wang, W., 2002. An improved in situ and satellite SST analysis for climate. J. Clim. 15, 1609–1625.
Risbey, J.S., Pook, M.J., McIntosh, P.C., Wheeler, M.C., Hendon, H.H., 2009. On the remote drivers of rainfall variability in Australia. Mon. Weather Rev. 137, 3233–3253.
Roxy, M.K., Ritika, K., Terray, P., Masson, S., 2014. The curious case of Indian ocean warming. J. Clim. 27, 8501–8509.
Rustic, G.T., Koutavas, A., Marchitto, T.M., Linsley, B.K., 2015. Dynamical excitation of the tropical Pacific Ocean and ENSO variability by Little ice age cooling. Science 350, 1537–1541.
Saji, N.H., Goswami, B.N., Vinayachandran, P.N., Yamagata, T., 1999. A dipole mode in the tropical Indian Ocean. Nature 401, 360–363.
Saji, N.H., Yamagata, T., 2003. Structure of SST and surface wind variability during Indian Ocean Dipole mode events: COADS observations. J. Clim. 16, 2735–2751.
Schott, F.A., Xie, S.-P., McCreary Jr., J.P., 2009. Indian Ocean circulation and climate variability. Rev. Geophys. 47 https://doi.org/10.1029/2007RG000245.
Sigl, M., Winstrup, M., McConnell, J.R., Welten, K.C., Plunkett, G., Ludlow, F., Büntgen, U., Caffee, M., Chellman, N., Dahl-Jensen, D., Fischer, H., Kipfstuhl, S., Kostick, C., Maselli, O.J., Mekhaldi, F., Mulvaney, R., Muscheler, R., Pasteris, D.R., Pilcher, J.R., Salzer, M., Schüpbach, S., Steffensen, J.P., Vinther, B.M., Woodruff, T.E., 2015. Timing and climate forcing of volcanic eruptions for the past 2,500 years. Nature 523, 543. https://doi.org/10.1038/nature14565.
Smith, T.M., Reynolds, R.W., Peterson, T.C., Lawrimore, J., 2008. Improvements to NOAA's historical merged land-ocean surface temperature analysis (1880-2006). J. Clim. 21, 2283–2296.
Stevenson, S., Fox-Kemper, B., Jochum, M., Rajagopalan, B., Yeager, S.G., 2010. ENSO model validation using wavelet probability analysis. J. Clim. 23, 5540–5547.
Stuecker, M.F., Timmermann, A., Jin, F.-F., Chikamoto, Y., Zhang, W., Wittenberg, A.T., Widiasih, E., Zhao, S., 2017. Revisiting ENSO/Indian Ocean Dipole phase relationships. Geophys. Res. Lett. 44, 2481–2492.
Taschetto, A.S., Gupta, A.S., Jourdain, N.C., Santoso, A., Ummenhofer, C.C., England, M.H., 2014. Cold tongue and warm pool ENSO events in CMIP5: mean state and future projections. J. Clim. 27, 2861–2885.
Taschetto, A.S., Gupta, A.S., Ummenhofer, C.C., England, M.H., 2016. Can Australian multiyear droughts and wet spells Be generated in the absence of oceanic variability? J. Clim. 29, 6201–6221.
Taschetto, A.S., Sen Gupta, A., Hendon, H.H., Ummenhofer, C.C., England, M.H., 2011. The contribution of Indian ocean sea surface temperature anomalies on Australian summer rainfall during El Niño events. J. Clim. 24, 3734–3747.
Thirumalai, K., DiNezio, P.N., Tierney, J.E., Puy, M., Mohtadi, M., 2019. An El Niño mode in the glacial Indian ocean? Paleoceanogr. Paleoclimat. 34, 1316–1327. https://doi.org/10.1029/2019PA003669.
Thompson, D.M., Ault, T.R., Evans, M.N., Cole, J.E., Emile-Geay, J., 2011. Comparison of observed and simulated tropical climate trends using a forward model of coral $\delta^{18}O$. Geophys. Res. Lett. 38 https://doi.org/10.1029/2011GL048224.
Thompson, D.M., Conroy, J.L., Collins, A., Hlohowskyj, S.R., Overpeck, J.T., Riedinger-Whitmore, M., Cole, J.E., Bush, M.B., Whitney, H., Corley, T.L., Kannan, M.S., 2017. Tropical Pacific climate variability over the last 6000 years as recorded in Bainbridge Crater lake, Galápagos. Paleoceanography 32, 903–922.
Thompson, L.G., Mosley-Thompson, E., Davis, M.E., Henderson, K.A., Brecher, H.H., Zagorodnov, V.S., Mashiotta, T.A., Lin, P.-N., Mikhalenko, V.N., Hardy, D.R., Beer, J., 2002. Kilimanjaro ice core records: evidence of Holocene climate change in tropical Africa. Science 298, 589. https://doi.org/10.1126/science.1073198.
Tierney, J.E., Abram, N.J., Anchukaitis, K.J., Evans, M.N., Giry, C., Halimeda Kilbourne, K., Saenger, C.P., Wu, H.C., Zinke, J., 2015a. Tropical sea-surface temperatures for the past four centuries reconstructed from coral archives. Paleoceanography, 2014PA002717.
Tierney, J.E., Oppo, D.W., Rosenthal, Y., Russell, J.M., Linsley, B.K., 2010. Coordinated hydrological regimes in the Indo-Pacific region during the past two millennia. Paleoceanography 25. https://doi.org/10.1029/2009PA001871.
Tierney, J.E., Smerdon, J.E., Anchukaitis, K.J., Seager, R., 2013. Multidecadal variability in east african hydroclimate controlled by the Indian ocean. Nature 493, 389. https://doi.org/10.1038/nature11785.
Tierney, J.E., Ummenhofer, C.C., deMenocal, P.B., 2015b. Past and future rainfall in the Horn of Africa. Sci. Adv. 1, e1500682.
Tourre, Y.M., White, W.B., 1995. ENSO signals in global upper-ocean temperature. J. Phys. Oceanogr. 25, 1317–1332.
Tyler, J.J., Mills, K., Barr, C., Sniderman, J.M.K., Gell, P.A., Karoly, D.J., 2015. Identifying coherent patterns of environmental change between multiple, multivariate records: an application to four 1000-year diatom records from Victoria, Australia. Quat. Sci. Rev. 119, 94–105.
Ummenhofer, C.C., Biastoch, A., Böning, C.W., 2017. Multidecadal Indian ocean variability linked to the pacific and implications for preconditioning Indian Ocean Dipole events. J. Clim. 30, 1739–1751.
Ummenhofer, C.C., England, M.H., McIntosh, P.C., Meyers, G.A., Pook, M.J., Risbey, J.S., Gupta, A.S., Taschetto, A.S., 2009a. What causes southeast Australia's worst droughts? Geophys. Res. Lett. 36, L04706.
Ummenhofer, C.C., Kulüke, M., Tierney, J.E., 2018. Extremes in East African hydroclimate and links to Indo-Pacific variability on interannual to decadal timescales. Clim. Dynam. 50, 2971–2991.

Ummenhofer, C.C., Sen Gupta, A., Taschetto, A.S., England, M.H., 2009b. Modulation of Australian precipitation by meridional gradients in east Indian ocean sea surface temperature. J. Clim. 22, 5597–5610.
Vance, T.R., Roberts, J.L., Plummer, C.T., Kiem, A.S., van Ommen, T.D., 2015. Interdecadal Pacific variability and eastern Australian megadroughts over the last millennium. Geophys. Res. Lett. 42, 129–137.
Verdon-Kidd, D.C., 2018. On the classification of different flavours of Indian Ocean Dipole events. Int. J. Climatol. 38, 4924–4937.
Wang, C., 2019. Three-ocean interactions and climate variability: a review and perspective. Clim. Dynam. 53, 5119–5136.
Wang, H., Kumar, A., Murtugudde, R., Narapusetty, B., Seip, K.L., 2019. Covariations between the Indian Ocean dipole and ENSO: a modeling study. Clim. Dynam. 53, 5743–5761.
Wang, Y., Cheng, H., Edwards, R.L., He, Y., Kong, X., An, Z., Wu, J., Kelly, M.J., Dykoski, C.A., Li, X., 2005. The Holocene asian monsoon: links to solar changes and north atlantic climate. Science 308, 854. https://doi.org/10.1126/science.1106296.
Weber, J.N., Woodhead, P.M.J., 1972. Temperature dependence of oxygen-18 concentration in reef coral carbonates. J. Geophys. Res. 77, 463–473.
Webster, P.J., Moore, A.M., Loschnigg, J.P., Leben, R.R., 1999. Coupled ocean-atmosphere dynamics in the Indian Ocean during 1997-98. Nature 401, 356–360.
Weller, E., Cai, W., 2013. Realism of the Indian Ocean Dipole in CMIP5 models: the implications for climate projections. J. Clim. 26, 6649–6659.
Wittenberg, A.T., 2009. Are historical records sufficient to constrain ENSO simulations? Geophys. Res. Lett. 36, L12702.
Yan, H., Wei, W., Soon, W., An, Z., Zhou, W., Liu, Z., Wang, Y., Carter, R.M., 2015. Dynamics of the Intertropical Convergence Zone over the Western Pacific during the Little Ice Age. Nat. Geosci. 8, 315.
Yuan, C., Tozuka, T., Luo, J.-J., Yamagata, T., 2014. Predictability of the subtropical dipole modes in a coupled ocean–atmosphere model. Clim. Dynam. 42, 1291–1308.
Zhao, Y., Nigam, S., 2014. The Indian Ocean Dipole: a monopole in SST. J. Clim. 28, 3–19.
Zheng, X.-T., Xie, S.-P., Du, Y., Liu, L., Huang, G., Liu, Q., 2013. Indian Ocean Dipole response to global warming in the CMIP5 multimodel ensemble. J. Clim. 26, 6067–6080.
Zhu, J., Liu, Z., Brady, E., Otto-Bliesner, B., Zhang, J., Noone, D., Tomas, R., Nusbaumer, J., Wong, T., Jahn, A., Tabor, C., 2017. Reduced ENSO variability at the LGM revealed by an isotope-enabled Earth system model. Geophys. Res. Lett. 44, 6984–6992.
Zinke, J., Dullo, W.C., Heiss, G.A., Eisenhauer, A., 2004. ENSO and Indian Ocean subtropical dipole variability is recorded in a coral record off southwest Madagascar for the period 1659 to 1995. Earth Planet Sci. Lett. 228, 177–194.
Zinke, J., Pfeiffer, M., Park, W., Schneider, B., Reuning, L., Dullo, W.C., Camoin, G.F., Mangini, A., Schroeder-Ritzrau, A., Garbe-Schönberg, D., Davies, G.R., 2014. Seychelles coral record of changes in sea surface temperature bimodality in the western Indian Ocean from the Mid-Holocene to the present. Clim. Dynam. 43, 689–708.
Zinke, J., Pfeiffer, M., Timm, O., Dullo, W.C., Davies, G.R., 2005. Atmosphere-ocean dynamics in the western Indian ocean recorded in corals. Phil. Trans.: Math. Phys. Eng. Sci. 363, 121–142.
Zinke, J., Pfeiffer, M., Timm, O., Dullo, W.C., Kroon, D., Thomassin, B.A., 2008. Mayotte coral reveals hydrological changes in the western Indian Ocean between 1881 and 1994. Geophys. Res. Lett. 35 https://doi.org/10.1029/2008GL035634.